SURFACE PATTERNING OF HIGHLY ORDERED PYROLYTIC GRAPHITE

A Thesis

Presented to the Faculty of the Graduate School

of Cornell University

in Partial Fulfillment of the Requirements for the Degree of

Master of Science

by

Bryan Hicks

May 2010

© 2010 Bryan Hicks

ALL RIGHTS RESERVED

ABSTRACT

A depth-controlled process for the tip-based etching of highly ordered pyrolytic graphite has been developed. This process provides unprecedented control on the dimensional parameters of the structures. Arrays of over 100 structures have been fabricated with strict tolerances on the placement, depth, and size of each feature. Custom software provides closed-loop depth control as well as the ability to change the fabrication parameters on-demand, immediately before each feature is made. To date, protrusions, holes, trenches, and even words have been patterned on scales ranging from 1 nm^2 to 1 mm^2 and depths ranging from sub nm to as deep as 200 nm. A 1.5 μm^2 array of 100 holes was fabricated. The average hole depth was 19.9 nm ± 2.2 nm and the average width was 32.2 nm ± 4.4 nm. Additionally, an array of 105 trenches with two different lengths was fabricated. The array was 3.2 µm across and 2.2 µm down. The pitch in the x direction was 350 nm and in the y direction was 155 nm. The two lengths present in the array had an average value of 136 nm for the short lines and 183 nm for the long lines with a variation of 4.4% and 2.7% respectively.

BIOGRAPHICAL SKETCH

Bryan Thomas Hicks was born in Falls Church, Virginia in 1984. He is the second of four brothers and a baby sister. Bryan was raised by loving parents who were surprised by his fascination with science but were nonetheless convinced he was their son. They enthusiastically helped him with his homework until letters began entering the equations. Undeterred, Bryan went on to graduate from Loveland High School in Ohio, study Physics at Brigham Young University in Utah and enter a PhD program in Electrical and Computer Engineering at Cornell University. His parents continue to support him with polite questions about his studies and he politely keeps his answers short. Bryan is married to his college sweetheart, a former History and ESL teacher who also prefers to keep her numbers and letters separate. They have a baby girl named Norah who is showing an early interest in technology. This work is dedicated to her in full confidence that she will one day understand it and even give her dad a hand with tricky equations from time to time.

To Norah

Love Daddy

ACKNOWLEDGEMENTS

I would like to acknowledge a few people, in particular, for their invaluable help and support. First, my advisor Clifford Pollock who wisely made me write this thesis in the first place. Clif has been a great motivator and advisor during my time here at Cornell. Secondly, I would be remiss if I did not acknowledge my fellow carbon-cutter, Norimasa Yoshimizu. He was always around to bounce ideas off of and helped me with every aspect of this project. He has been like a secondary advisor to me and we shared several all nighters– just him, me, and the AFM. Lastly, I would like to acknowledge my wonderful wife Lindsey who was always understanding when I spent more time with Nori than I did with her.

TABLE OF CONTENTS

Biographical Sketch . . . iii
Dedication . . . iv
Acknowledgements . . . v
Table of Contents . . . vi
List of Tables . . . viii
List of Figures . . . ix

1 Introduction **1**
1.1 Overview . . . 1
1.2 Highly Ordered Pyrolytic Graphite . . . 2
1.2.1 What is HOPG? . . . 2
1.2.2 Graphene: Single-layer HOPG . . . 5
1.2.3 Applications of HOPG . . . 5
1.3 Surface Patterning of HOPG . . . 6
1.4 The Atomic Force Microscope (AFM) . . . 7

2 Mechanism for Tip-based Etching of HOPG **11**
2.1 Previously Proposed Mechanisms . . . 11
2.2 Necessary Criteria of a Viable Mechanism . . . 12
2.3 HOPG Etching Mechanism . . . 16
2.3.1 Polarity Dependence . . . 16
2.3.2 Bias Voltage Dependent Behavior . . . 16
2.3.3 Negligible or No Current Required . . . 17
2.3.4 Meniscus Necessary Between Tip and Sample . . . 18
2.3.5 Liquid Residue Surrounding Etched Features . . . 18
2.3.6 Unpredicted Carbon Deposition . . . 19

3 Methods **20**
3.0.7 Tip Preparation . . . 20
3.0.8 HOPG Preparation . . . 21
3.0.9 AFM Settings and Operation . . . 22
3.0.10 LabVIEW-AFM Interface . . . 25
3.1 Fabrication . . . 28
3.1.1 Holes . . . 28
3.1.2 Trenches . . . 29
3.1.3 Arrays . . . 31
3.1.4 Hysteresis . . . 33
3.1.5 Tip Cleaning . . . 33
3.2 Imaging . . . 34
3.3 Measuring . . . 35

4 Results **36**
4.1 Holes and Arrays of Holes 36
4.2 Trenches and Arrays of Trenches 38

5 Discussion **42**
5.1 Effect of Etch Rate on Feature Quality 42
5.2 Temperature Dependence 42
5.3 Conclusion 44

A Troubleshooting **46**
A.1 No Etch Even at High Voltages 46
A.2 Z Piezo Drift 46
A.3 X,Y Piezo Issues 47
A.4 Coupling of Channel Signals 48
A.5 Etch Stops During Fabrication of Large Array 48

B LabVIEW Program **49**

Bibliography **75**

LIST OF TABLES

4.1 Hole Fabrication Parameters 36
4.2 Trench Fabrication Parameters 38

LIST OF FIGURES

1.1 STM image of graphite 2
1.2 HOPG atomic structure 3
1.3 Laser beam deflection for AFM tip sensing 8
1.4 Parameters dial 10

2.1 Polarity dependence of HOPG etching 13
2.2 Etch rates for different bias voltages 13
2.3 Measured current during etching 14
2.4 Water residue formed by etching 15

3.1 AFM tip dimensions 20
3.2 SEM images of an AFM tip at various stages 22
3.3 Loading of HOPG into AFM 23
3.4 Knobs used in AFM setup 24
3.5 Relating distances measured in voltages to distances in nm . . . 27
3.6 Hole etched in HOPG 29
3.7 Hole width as a function of depth 30
3.8 Trench etched in HOPG 31
3.9 Comparison of scanning techniques 32
3.10 Reverse bias as an effective tip cleaning method 34
3.11 Method for measuring line length 35

4.1 10 x 10 array of holes etched in HOPG 37
4.2 Distributions of hole depths and diameters 37
4.3 105 features arranged in a 7x15 array 39
4.4 Distributions of lengths for short and long lines 39
4.5 Profile of short and long line 40
4.6 Distribution of depths for etched lines 40

5.1 Temperature dependence of HOPG etching process 43

B.1 LabVIEW front panel 50
B.2 Loop 1 51
B.3 Loop 2 52
B.4 Loop 3 53
B.5 True/False loop (False Case) 54
B.6 True/False loop (True Case) 55
B.7 Code inside true case of loop 3 56

CHAPTER 1

INTRODUCTION

1.1 Overview

An automated process for on-the-fly pattering of highly ordered pyrolytic graphite (HOPG) is presented. This process utilizes a commercial atomic force microscope (AFM) system which is controlled by custom software. The custom software provides closed-loop depth control as well as the ability to change the fabrication parameters on-demand.

In this thesis the materials, instruments, techniques and theories which underlie this HOPG etching process are thoroughly explained. The synthesis, properties, and applications of the major material involved, HOPG, are outlined. An introduction to AFM systems and their use in the surface patterning of HOPG is given along with other surface patterning methods. The setup, fabrication, and post-processing steps are explained in detail for the fabrication of both holes and trenches. The custom software implemented is explained and its purpose justified. Proposed HOPG etching mechanisms are explored and a viable mechanism along with supporting evidence is presented. Lastly, the applications of this HOPG etching process are presented along with further work to be done in the field.

1.2 Highly Ordered Pyrolytic Graphite

1.2.1 What is HOPG?

Highly ordered pyrolytic graphite or HOPG is a special class of graphite that can be described effectively by a decomposition of its name.

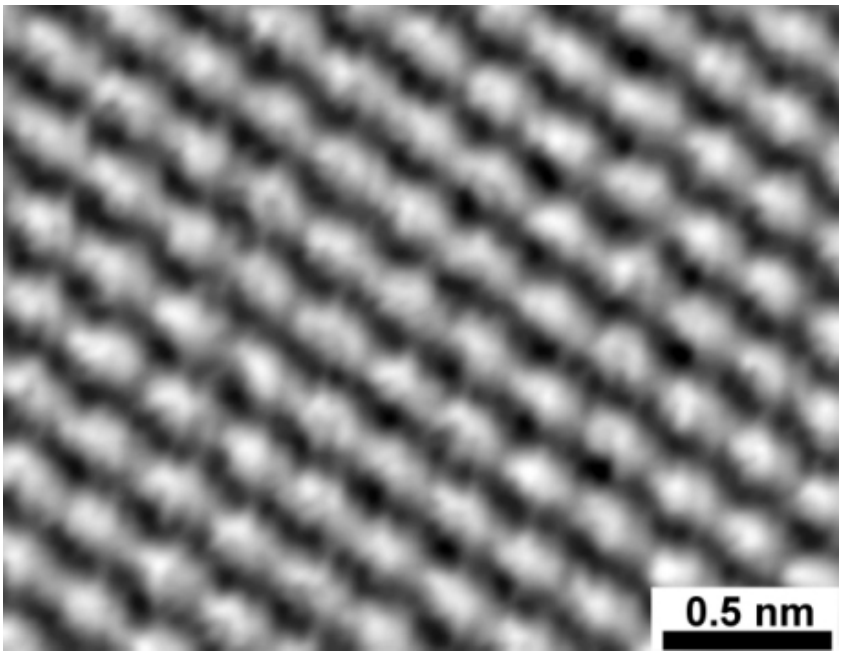

Figure 1.1: STM image of graphite.

HOPG can be most closely modeled by the ideal *graphite* structure. HOPG is a stack of sp^2-bonded carbon atom planes with a hexagonal crystal structure and an -ABAB- stacking sequence (See Figure 1.2). HOPG's elasticity (See equation (1.1) is highly anisotropic and so layers of the carbon planes easily peel off in sheets (similar to Mica). The interplane elasticity is 36.5 GPa whereas the intraplane elasticity is 1060 GPa [1]. This large anisotropy makes it possible to achieve graphite monolayers, called graphene, by a Scotch tape cleaving process [1]. This cleaving process involves applying tape to the top surface of the

HOPG and then carefully removing it. It is important that the tape is not flexed in the process of removing it– the tape should be lifted straight up from the sample. Repeating this process on the removed layer can eventually result in a graphene layer.

$$E = \frac{F/A_o}{\Delta L/L_o} \tag{1.1}$$

- E is the Young's modulus
- F is the applied force
- A_o is the cross-sectional area over which the force is applied
- ΔL is the change in length
- L_o is the original length

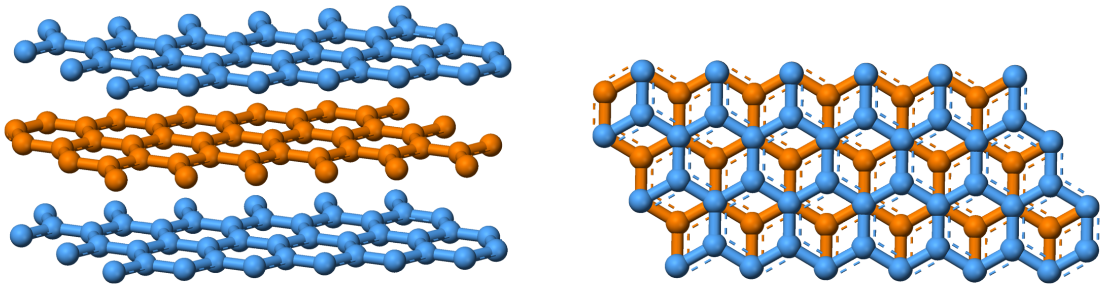

(a) Schematic showing planar stacking of HOPG.

(b) Top view schematic showing the hexagonal structure of HOPG and specifically illustrating -ABAB- stacking sequence.

Figure 1.2: Schematic showing the atomic structure of HOPG from a top and side view.

HOPG is made by means of a *pyrolytic* process. Pyrolysis is the chemical decomposition of organic material using heat. Pyrolysis occurs spontaneously

at high temperatures and can take place with or without the presence of oxygen or other reagents. In the case of HOPG a certain carbon containing material is heated to its decomposition temperature, the liberated atomic carbon deposits and recrystallizes on a suitable substrate. The carbon-containing material is generally a hydrocarbon-rich gas, most commonly CH_4, and pyrolysis is accomplished in a chemical vapor deposition (CVD) furnace. The result is a stack of highly planar graphene sheets, known as HOPG (See Figure 1.2). [2]

HOPG is *highly ordered*. Most graphite is poly crystalline and consists of numerous micron scale grains without consistent orientation and is riddled with defects of all sorts. HOPG has significantly fewer and much larger grains that have planar order rather than being randomly oriented. Commercially available HOPG is classified into different grades based on how ordered the sample is. The measure of this order is determined by X-ray diffraction. X-ray diffraction is a technique for determining crystal structure by studying interference patterns from planes of atoms. The position of the interference peaks as well as their widths provide information about the structure of the sample. Crystals with fewer defects and longer range order have narrower diffraction peaks, so the width of the peak is an indication of the quality of the crystal. The order of HOPG samples is reported as the mosaic spread of the sample. Mosaic spread refers to the full width at half maximum (FWHM) of one of these peaks, the Cu-K_α peak, which broadens with disorder. A smaller angle indicates larger grain sizes and fewer defects. Commercially available HOPG is classified in to three grades:

1. SPI-1 or ZYA (0.4° +/- 0.1°) mainly used for calibration
2. SPI-2 or ZYB (0.8° +/- 0.2°) used for most research

3. SPI-3 or ZYH (3.5° +/- 1.5°) for non-critical or instructional use

Each of these grades contains no more than 10 impurities per million carbon atoms and vary only in the number of defects and average grain size. [3]

1.2.2 Graphene: Single-layer HOPG

Graphene, ideally, is a single layer of graphite. Graphene is a popular and sought after material for its electronic and mechanical properties. It is ambipolar meaning both holes and electrons can serve as carriers in the material. Graphene exhibits ballistic transport on the micron scale eliminating loss due to heat. Graphene's Young's modulus is one of the highest of any known material at 1.2 TPa and graphene's mechanical and electronic properties are coupled by a highly responsive change in conductivity as a result of strain. Graphene sheets measuring 400 μm^2 can be obtained from HOPG utilizing the tape cleaving method described above. [4]

1.2.3 Applications of HOPG

In addition to graphene-related applications HOPG has several applications in its own right. It is widely used as a calibration sample for AFM systems because of its extremely flat surface [3]. It is the most efficient material known for the diffraction of both X-rays and neutrons and so is used in conjunction with these systems [3]. It has recently been used as a substrate for basic science investigations of DNA as well as for biosensors [5]. HOPG has been used as a nanoresonator and theorized to be capable of single atom mass detection because of its

extraordinarily large elasticity. It can also be used in atomic electromechanical systems, systems used for detecting quantum phenomena [6].

1.3 Surface Patterning of HOPG

Several methods have been successfully used to pattern the surface of HOPG samples.

1. Oxygen plasma etching of structures defined by conventional lithography. This technique is limited to the resolution achievable by current lithographic capabilities. It is not as readily flexible as the other two methods. [7].
2. Ablation of the HOPG surface through the use of pulsed excimer lasers. The resolution of this method is determined by the diffraction limit of the excimer laser, typically 300 nm. [8].
3. Tip-based (AFM [9, 10, 11, 12, 13] or STM [14, 15, 16, 17]) etching techniques using voltage pulses like the method detailed in this paper. These methods have the smallest limit on feature size and are very flexible, with the ability to make run-time modifications.

The first two presented here are very different approaches than the one presented in this thesis. The last item represents many variations of the same basic technique employed in the research described here. Tip-based methods have significant advantages in resolution and flexibility which ultimately led to the decision to pursue this type of approach.

1.4 The Atomic Force Microscope (AFM)

The atomic force microscope is an adaptation of the scanning tunneling microscope (STM), which measures changes in tunneling current between tip and substrate. The main advantage of the AFM over the STM is its ability to image insulating surfaces using either conducting or non-conducting tips. The atomic force microscope works by measuring tip deflection and from that calculating the force between the tip and the sample. Several different methods are used to measure tip deflection, including: tunneling detection, capacitance detection, optical interferometry and laser beam deflection. Due to the overwhelming popularity of this last approach, only laser beam deflection will be explained here. Additionally, there are two basic modes of operation for an AFM: *contact* and *non-contact*.

Laser beam deflection is a simple yet effective technique for measuring tip displacement. Figure 1.3 shows how a laser is focused on the back of the cantilever ($1600\,\mu m^2$) and reflected onto a quadrature photodiode about 4 cm away to detect tip deflections. Displacement is measured by calculating the difference in intensity between the top and bottom diodes and the left and right diodes for detecting vertical and torsional displacement, respectively. Angstrom resolution is routinely achieved using laser beam deflection. Advantages of this method over others include its: ease of implementation, minimal effect on measurement, robustness to environmental conditions, and cost. Some tip displacement detection techniques can significantly affect the measurement by the very process of measuring. Laser beam deflection, as listed, has a minimal effect on the measurement itself. This is one of the major reasons for its widespread use.

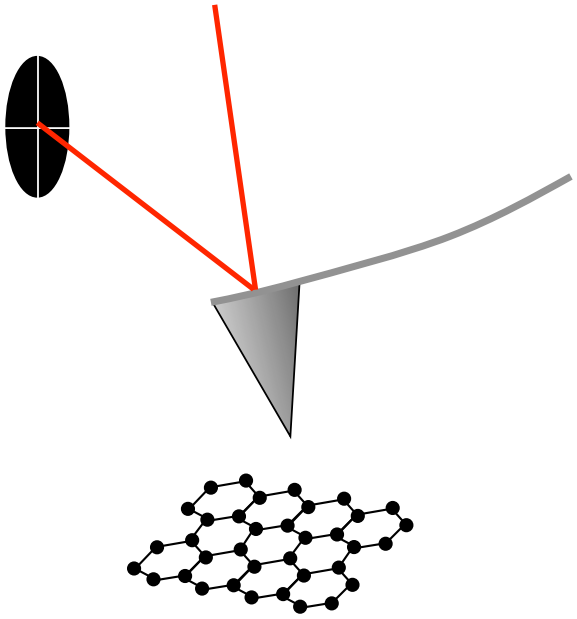

Figure 1.3: Laser beam deflection for AFM tip sensing. Laser is shown reflecting off the back of an AFM cantilever and incident on a quadrature photodiode. The differences in current between the top and bottom diodes is used to detect vertical deflection of the AFM tip.

Non-contact mode is accomplished by bringing the tip between 10-100 nm above the surface. The tip is generally driven at a frequency slightly off its resonant frequency with tip displacement amplitudes ranging from 1-10 nm. The tip is then scanned over the sample surface or in many cases the tip is held still and the sample is moved underneath the tip. In this mode the longer range forces such as van der Waals forces, electrostatic and magnetic dipole forces dominate over shorter range forces like ion-ion repulsion.

In contrast, the major force measured in contact mode is the repulsion between the positive ion cores of the tip and the sample. The other longer range forces are not as significant. This is because in contact mode the tip is brought ¡¡10nm above the surface of the sample. At this range wavefunctions are overlapping and causing repulsion. These forces have a strong tip-sample spacing

dependence. A topographic image obtained in contact mode will show the locations of the atom nuclei rather than the electron density which is more likely to be obtained in non-contact mode.

The mode used here in patterning the substrate is a contact, constant force mode. This means that the tip will be very close to the sample surface and as the sample surface is scanned below the unmoving tip a constant force is maintained between the tip and the substrate by actuating a piezoelectric stack attached to the sample stage. This piezoelectric transducer will move the sample closer or farther from the tip to maintain a constant force. Topographic images can be obtained in this mode by mapping the voltage applied to the z axis PZT as a function of x and y. [18]

The specific AFM system used in this research is a JEOL SPM-4200. This system uses laser beam deflection to measure tip displacement and can be operated in either contact or non-contact mode. The AFM tip is held stationary in the tip holder located in the head of the machine. The tips used in this experiment are platinum-coated, conducting AFM tips. There are 4 indicators used to align the laser to the cantilever of the AFM tip: SUM, AFM, FFM, RMS. These 4 indicators are explained below:

1. **SUM** displays the combined voltage of the quadrature photodiode. This value helps to ensure that the majority of the laser beam is incident on the diodes.
2. **AFM** displays the combined voltage of the top 2 diodes subtracted from the combined voltage of the bottom two diodes.
3. **FFM** displays the combined voltage of the left 2 diodes subtracted from the combined voltage of the right two diodes.

4. **RMS** displays a voltage directly related to the peak amplitude of the cantilever. (This is used only in non-contact mode).

These voltages are displayed by turning the dial pictured in Figure 1.4 to the appropriate setting.

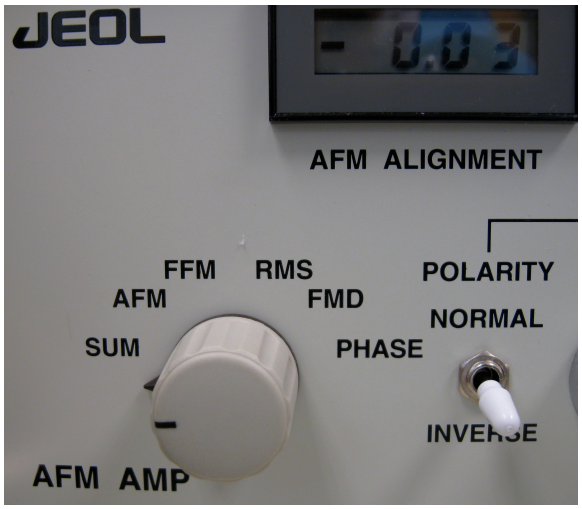

Figure 1.4: This dial is used to display the SUM, AFM, FFM and RMS parameters which are used in aligning the laser to back of the cantilever of the AFM tip. Each of these parameters can be modified using physical knobs or changing setting using the SPM-scanning software.

Each of these values can be modified by turning particular knobs located on the head of AFM or by using the SPM-scanning software. A description of how to modify each of them is given in Section 3.0.9 where the procedure for aligning the laser to the back of the AFM tip's cantilever is explained.

CHAPTER 2

MECHANISM FOR TIP-BASED ETCHING OF HOPG

Several different theories have been proposed for how HOPG is etched and many others have been eliminated, but no mechanism is completely agreed upon. This section will explore several candidates that have been eliminated and the necessary criteria for a valid HOPG etching mechanism.

2.1 Previously Proposed Mechanisms

Mechanical: Gold and other materials can be etched mechanically by scratching the surface with an AFM tip [19]. This mechanism was eliminated as a possible candidate for HOPG etching because even when the tip was pressed 100 nm into the HOPG surface no indentation was made [14].

Thermal: The evaporation of graphite as a result of local heating has also been eliminated as a potential mechanism. Theoretical work suggests that it is unlikely that the necessary temperatures could be reached, especially considering that metal-coated tips are employed [20]. This work, however, is based on a macroscopic calculation which may not be viable at these small scales. Although the theory may be flawed, experiments have demonstrated that the heat necessary for carbon evaporation is not generated during the HOPG etching process. Metal coated tips, resulting in high thermal conductivities, are used in HOPG etching and these tips dissipate the heat too quickly for any substantial local heating to take place [10].

Current Driven: Field-emission [21, 22] and tunneling electrons [10] along with

electron-induced reactions [17] have also been proposed as possible mechanisms. None of these mechanisms can explain the etching process in the case where the currents are in the picoamp range compared to the predicted microamp range. The proper mechanism will account for carbon etching without relying on an electron-mediated process.

2.2 Necessary Criteria of a Viable Mechanism

In order for an etching mechanism theory to be viable it must explain the following observed characteristics:

Polarity dependence HOPG etching only occurs when a positive sample bias is applied (See Figure 2.1). This same requirement has been reported nearly unanimously throughout the literature [12, 10, 13, 11, 9, 17, 14, 15]. The only exception reported, claims that carbon nanotubes can be cut using an STM regardless of the applied bias polarity [16].

Bias voltage dependent behavior In addition to being dependent on the voltage polarity the magnitude of the applied bias also effects the results. For voltages smaller than 4 V, protrusions around 1-2 nm above the HOPG surface are observed rather than concave pits as reported in the literature [12, 11]. As the voltage is increased protrusions are no longer observed, even for short processing times. The etch rate is constant over time at a particular voltage but increases with increasing applied bias. This increase in etch rate seems to level off at higher voltages and at voltages above 15 V the process is inconsistent and unpredictable.

Negligible or no current required The current measured during etching is in

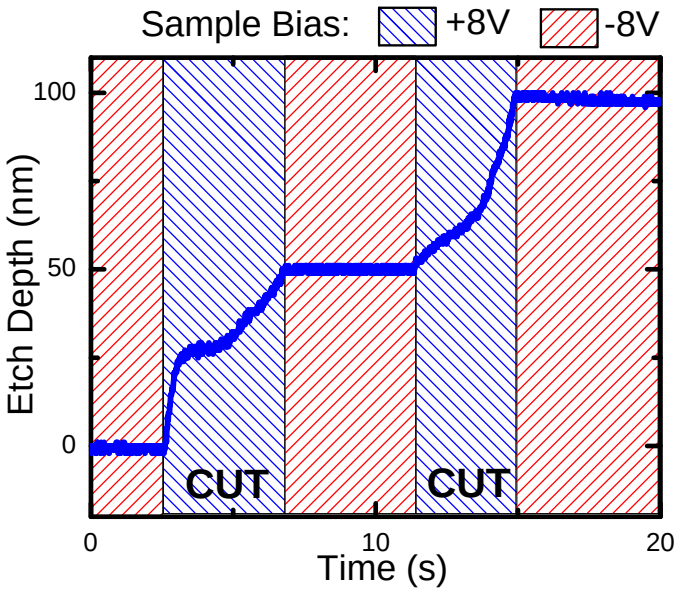

Figure 2.1: HOPG etching occurs only for positive sample bias voltages

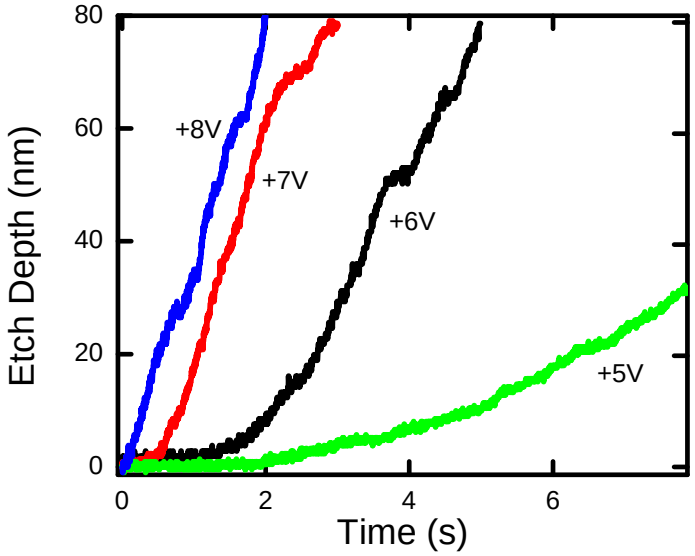

Figure 2.2: Etch rates for different bias voltages

the picoamp range and when low voltage and high currents are applied no etching occurs. This behavior has also been seen and tested by Park et al. and Jiang et al [10, 13]. The only group that reports significant current during the etching process is the Dal-Hyun Kim group and this was in the case of cutting multi-walled carbon nanotubes, which may or may not be applicable to HOPG etching [22].

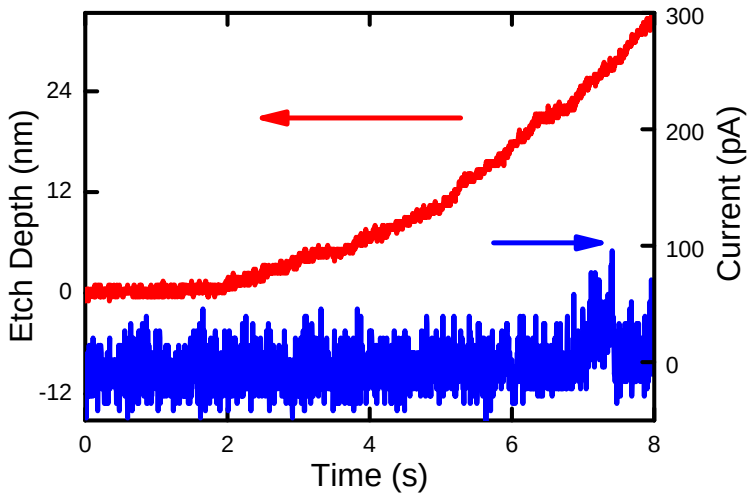

Figure 2.3: The change in tip height is plotted above while the measured current during the etch is plotted below

Meniscus necessary between tip and sample This requirement also imposes other experimental limitations. In order for a meniscus to form between the tip and sample a layer of water must adsorb on the HOPG surface. For this to happen the sample must be exposed to an environment with a certain threshold humidity. We measured this humidity threshold to be around 40%, while this figure varies, numerous groups report that the process is humidity dependent [12, 22, 10, 13, 11]. Thus, etching cannot occur under vacuum or in environments devoid of ambient water vapor as confirmed by Park et al. and Jiang et al [10, 13].

A good indicator that a meniscus has been formed is a characteristic asymmetry in tip displacement as a function of the AFM reference voltage. If a meniscus has formed between the tip and sample only small changes in tip displacement will be seen as the tip is moved away from the surface. This occurs because the tip is being held by the water meniscus. At a certain point the flex in the cantilever will become too great and the tip will break free from the meniscus and a discontinuous jump in tip position will be observed. If the reference voltage is subsequently increased the tip position will increment steadily back towards the same position and not exhibit this behavior.

Liquid residue surrounding etched features Although not reported in the literature, water is visible surrounding the etched features (See Figure 2.4 a). This fine structure was confirmed to be water by pumping down the chamber to vacuum, when the same area is imaged under vacuum the structure is no longer present. (see Fig. 2.4 b).

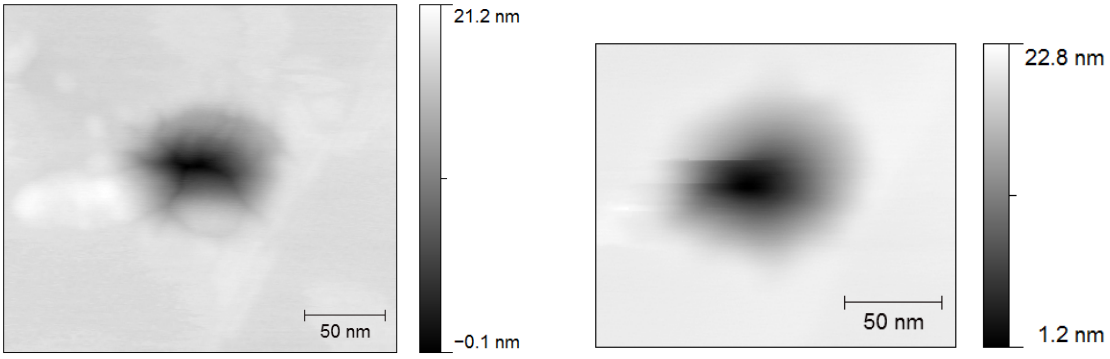

(a) Tapping mode topographic AFM scan with water evident on HOPG surface

(b) Contact mode scan in which the water on the surface is no longer visible

Figure 2.4: The etching process often results in a water residue surrounding the etched feature. This residue is only seen in the tapping mode scan and not in the contact mode scan.

2.3 HOPG Etching Mechanism

The process of graphite etching is assumed to be due to an aqueous electrochemical oxidation and removal of the surface carbon atoms. The main graphite etching reaction is the generation of carbon dioxide [23, 15, 24]. This reaction meets all the criteria necessary to explain the observed behavior.

$$C + 2H_2O \quad \rightleftharpoons \quad 4H^+ + 4e^- + CO_2, \tag{2.1}$$

2.3.1 Polarity Dependence

The above reaction is an irreversible reaction which has a region of stability for positive sample voltages. This is best illustrated by the Pourbaix diagram for carbon (See Appendix) [25]. Under reverse bias reverse polarities, the Pourbaix diagram also predicts a stable carbon etching reaction. This reaction results in the generation of methane but requires four hydrogen ions and four free electrons. Although it cannot be deduced from the diagram, this is a highly improbable reaction. This explains why a strict polarity dependence is seen in the HOPG etching process.

2.3.2 Bias Voltage Dependent Behavior

Through a combination of information found in the Pourbaix diagram and chemical kinetics the bias voltage dependence of the HOPG etching process can be readily explained. For positive sample biases the Pourbaix diagram predicts

stable reactions for both graphite oxidation and etching. When chemical kinetics are accounted for it can be shown that oxidation is favored at small voltages and etching at large voltages. This explains why small protrusions are seen on the HOPG surface at voltages less than 4 V but above this threshold only etching is observed. In addition, the rate of equation (2.1) increases at higher sample voltages, resulting in higher etch rates at these voltages.

Another important feature of the applied voltage dependence is that the constant-voltage etch rate is unchanging as a function of time. The amount of solvent involved in this reaction is very small so its molal ionic strength (a measure of ion concentration weighted by charge) can be easily changed. Even with the small amounts of carbon involved the molal ionic strength of the remaining solvent should increase dramatically according to equation (2.1). Since the molal ionic strength strongly affects the rate of reaction, the etch rate should change by orders of magnitude as a function of time even if the voltage is constant. The reason that this is not observed is because the hydrogen ions and the free electrons readily combine and are released as hydrogen gas.

2.3.3 Negligible or No Current Required

In contrast to many of the proposed reactions referenced above, Equation (2.1) does not require electrons in order to occur. Additionally, because the resulting hydrogen ions and free electrons readily combine and are dissipated as hydrogen gas minimal current is predicted. This feature closely resembles what is observed in experiment. Only at larger voltages, where these ions and electrons are strongly attracted to the tip and substrate, respectively, is a measurable cur-

rent predicted.

2.3.4 Meniscus Necessary Between Tip and Sample

The water necessary for (2.1) to occur comes from the meniscus that forms between the carbon surface and the scanning probe tip. This explains why HOPG etching does not occur under vacuum. An adsorbed water film is present on graphitic surfaces even at humidities as low as 15% and this layer increases in thickness with increasing humidity [26]. This explains why varying humidity thresholds have been reported. Meniscus formation is easier at higher relative humidities, but it is possible across a wide range of humidities.

2.3.5 Liquid Residue Surrounding Etched Features

The presence of water on the HOPG surface is not expected because graphite is hydrophobic. The reason that water is found after the etching process requires a two-part answer. First, applying a positive bias to the carbon sample can result in etching but it can also result in oxidation. Graphene oxides, as opposed to carbon, are hydrophillic which would contribute to the increased wettability of the surface [27]. Secondly, graphite's wettability may also be raised by an increased acidity caused by the formation of carbonic acid and carbonates also predicted by the carbon Pourbaix diagram.

$$C + 3H_2O \rightleftharpoons H_2CO_3 \tag{2.2}$$

$$C + 3H_2O \rightleftharpoons HCO_3^- + H^+ \tag{2.3}$$

$$C + 3H_2O \rightleftharpoons CO_3^{--} + 2H^+ \tag{2.4}$$

2.3.6 Unpredicted Carbon Deposition

One unexpected feature observed during the etching process is the accumulation of carbon on the AFM tip. Energy dispersive x-ray spectroscopy with an electron beam microprobe was used to confirm the deposited material to be carbon and techniques discussed in 3.1.5 are applied to mitigate the problem, but a good explanation for why it occurs is still unclear. According to equation (2.1) the etch should happen cleanly, without carbon build up. However after several hundred hole etches, without mitigation, the deposited carbon is clearly visible in an SEM image of the tip.

CHAPTER 3

METHODS

The setup includes an atomic force microscope system using platinum-coated tips and controlled via an external program. The tips are prepared before hand to improve their durability and reliability. The HOPG is cleaved and loaded into the system. The AFM is setup and then controlled by a custom program for the fabrication process. Imaging is done using the AFM and the same tip used for fabrication.

3.0.7 Tip Preparation

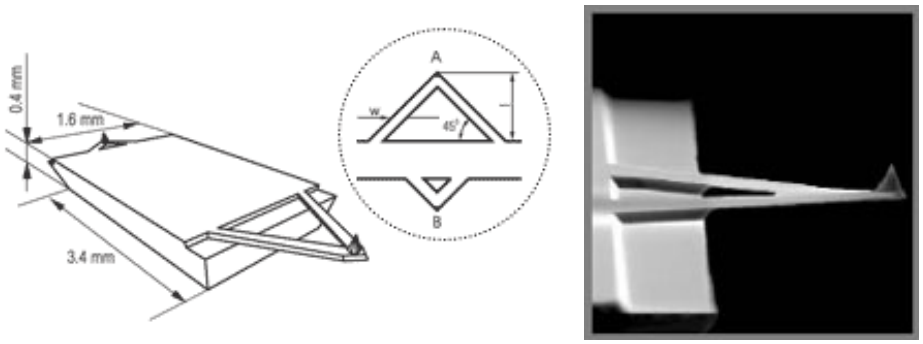

(a) Schematic of AFM tips used

(b) An SEM image of an AFM tip like those used in the presented research.

Figure 3.1: An SEM image of an AFM tip like those used in the presented research. This image is available from the AFM tip manufacturer.

The AFM tips used are commercially-available, platinum-coated, silicon tips (Mikromasch CSC11/Pt). AFM tips consist of three components, usually etched out of a single piece of silicon: the probe chip, the cantilever, and the tip itself. The probe chip is 1.6 mm by 3.4 mm and acts as a holder for the cantilever and

tip. The cantilever in this case is consists of 2 beams connected to form a triangle and each leg of the triangle meets the probe chip at 45°. The height of the triangle is 200 µm, the width of each leg is 40 µm and it is 1 µm thick. At the apex of the triangle a tip is located. The tip has a conical shape and descends 20-25 µm below the cantilever. The end of the tips is made to be as sharp as possible to provide good resolution. The initial tip radius of the platinum coated tips is 25 nm. A major issue in using AFM tips in contact mode is wear on the sharp point as the tips tend to become less sharp with use. This change in the tip surface and geometry can lead to inconsistent etching. To address this issue, the tips are blunted prior to use by repeated scanning along an HOPG surface using the AFM in contact mode. Twenty raster scans over a 500 nm^2 area is sufficient to blunt the tips to a radius of approximately 50 nm. Once the tips are blunted they are more resilient to further deformation. This results in more consistent etches because the tip shape is more constant throughout the procedure. Additionally blunted tips more reliably etch the HOPG surface because they more easily form a meniscus between the tip and the surface. This is a requirement of the mechanism responsible for tip-based etching of HOPG, which is discussed in greater detail in section 2.3.

3.0.8 HOPG Preparation

A thin film of research grade HOPG (200 nm) is adhered to a piece of double-sided copper tape and then attached to the stage mount. This is accomplished by firmly pressing a piece of copper tape against the surface of a 10 x 10 x 2 mm sample of HOPG. The tape is removed at a slow, constant speed, while minimizing any bending of the copper tape. Once a flat HOPG surface, with minimal

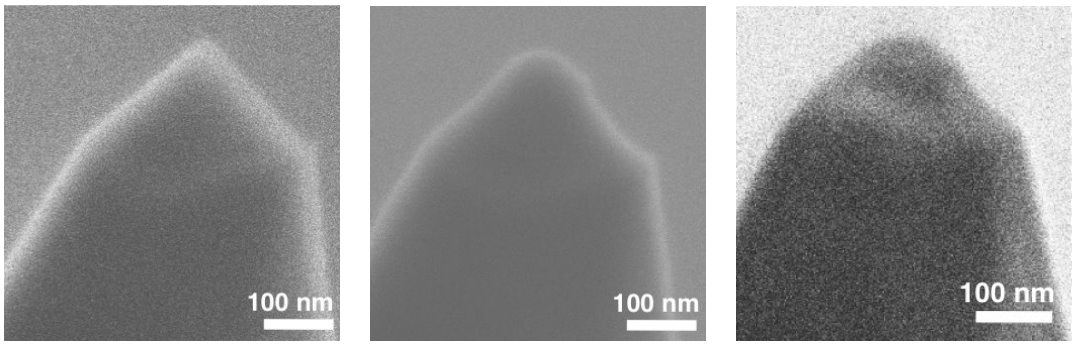

(a) A scanning electron microscope (SEM) image showing tip shape and size prior to any processing

(b) SEM image of the same tip after 20 contact-mode scans over a 500 nm^2 area

(c) SEM image of the same tip after etching 60 holes in HOPG sample

Figure 3.2: SEM images of an AFM tip at various stages

protruding flakes of graphite, is achieved it is attached to the AFM stage mount using the other adhesive side of the copper tape (see figure 3.4). Copper tape is used because it is conductive and so the sample can be easily biased, it is also double-sided so it can be used to both cleave and mount the sample. The bottom and the two sides of the stage mount which will be in contact with the mount holder are then covered in an electrically isolating tape (not the copper tape). This tape can be seen on the front side of the stage mount in figure 3.3(a). Figure **??** show the two sides of the holder in contact with the stage mount. These sides must be electrically isolated from the stage. This allows the HOPG sample to be biased with respect to the tip. The stage mount is then loaded into the AFM system and wires are connected to the stage to apply bias voltages.

3.0.9 AFM Settings and Operation

The tip is carefully loaded into the tip holder in the head of the AFM ensuring that it sits flush and square against the back of the tip mount. Once this is ac-

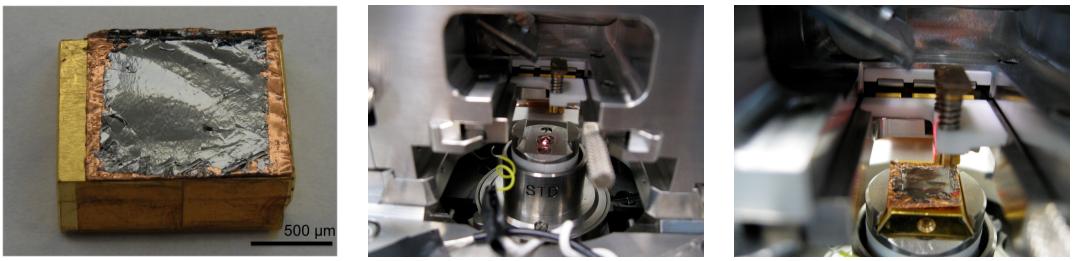

(a) HOPG Sample mounted on AFM stage mount. Although the sample looks very rough it is locally flat. A typical grain size for HOPG is about 10 μm^2. Over regions this size the HOPG is atomically flat.

(b) AFM head without HOPG sample. Note the laser which is used for detecting tip deflection.

(c) AFM head with mounted HOPG sample loaded

Figure 3.3: Different stages of preparing and loading an HOPG sample into the AFM

complished the laser must be aligned to the back of the cantilever. The JEOL SPM-4200 has 4 knobs that are used in this alignment: AFM, which affects the voltage difference between the top and bottom photodiodes, turning this knob moves the quadrature photodiode up and down; FFM, which affects the voltage difference between the left and right photodiodes, turning this knob moves the quadratures photodiode left and right; X, which moves the laser beam in the x direction (perpendicular to height of the triangular cantilever); and Y, which moves the laser beam in the y direction (parallel to the height of the triangular cantilever). The position of each of these knobs is shown in figure 3.4. Another parameter used in the alignment process is SUM, which is the total signal from the 4 photodiodes. The alignment procedure is accomplished using these 4 knobs in the following manner:

1. Roughly align the laser to the tip-end of the cantilever using the optical scope. The laser should be visible on the HOPG surface and can be moved using the x and y knobs until it is incident on the back of the cantilever.

2. Maximize SUM (SUM is the total signal from the 4 photodiodes) by moving the laser in the x direction. This will horizontally center the deflected beam on the quadrature photodiode.

3. Move the laser in the y direction until a SUM value of 3 V is reached. Limiting the SUM value to 3 V helps to ensure that the laser is focused toware the tip of the cantilever rather than closer to the probe chip.

4. Adjust the AFM knob (moves the quadrature diode up and down) using large dial on side to −2.7 V.

5. Adjust FFM knob (moves the quadrature diode left to right) using front dial on head to 0.

6. Iterate steps 2 through 5 until FFM= 0 and AFM= −2.7 and SUM> 3

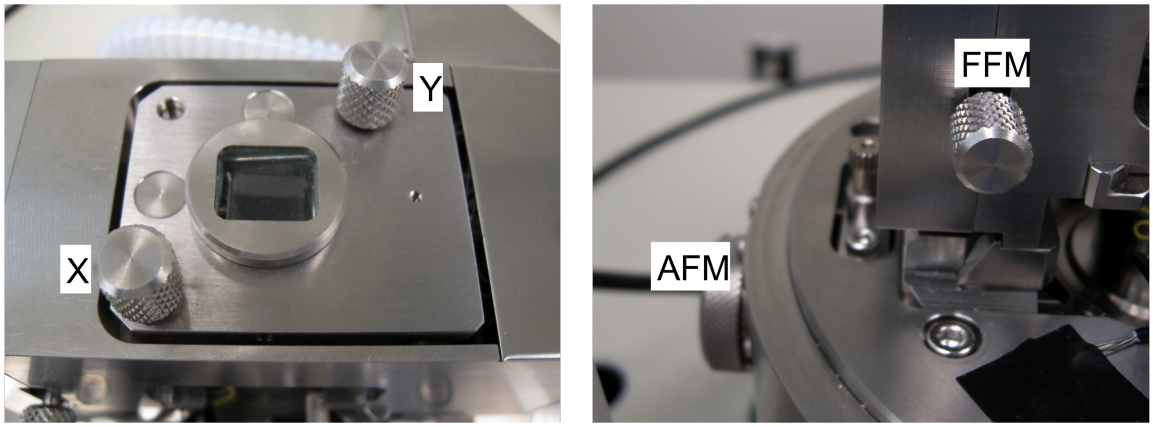

(a) X and Y knobs used for aligning laser to the back of the cantilever.

(b) AFM and FFM knobs used to adjust the position of the quadrature photodiode

Figure 3.4: The placement of the four knobs used for aligning the laser to the back of the cantilever.

Once the laser is aligned to the back of the cantilever the rest of the AFM settings must be made in the SPM parameters window. The Advanced tab must be used for this portion because the preconfigured modes do not provide enough

options. The STM/AFM must be set to *slope*, which is the non-contact mode, for the following steps. First, the resonant frequency of the tip is determined by a VCO scan. The frequency at which the tip is driven is then tuned within 0.5 Hz of this frequency and the Output Amp/ V is adjusted so that the RMS value is approximately 4 V.

The tip can now be brought in contact with the sample. While the AFM is still in slope mode lower the tip until topographic images with a total height difference less than 5 nm are obtained. The AFM is now switched to contact mode and the sample is approached slowly once again until the tip is in contact with the sample. This is determined again by monitoring the total height difference across a topographic scan of the surface. Doing the initial approach in tapping mode minimizes tip damage. Once the tip is in close proximity to the sample the final approach can safely be made in contact mode. Various voltages, from 4-10 V, are then applied to the sample, using the commercial software, to ensure that etching occurs and to optimize the bias voltage.

3.0.10 LabVIEW-AFM Interface

After this initial setup the rest of the process was done entirely through custom LabVIEW software. LabVIEW is a visual programming environment commonly used for data acquisition and instrument control. The primary reason for implementing this external control was because consistent etch depths could not be obtained by only controlling the time of the etch. For a depth variation of 10% the etch time varied 83%. With this amount of variation, it would be impossible to control the etch depth by only controlling the etch duration. Our custom soft-

ware was implemented in order to achieve greater depth uniformity by using a feedback control loop. The software reads the current voltage on the z-axis PZT and terminates the etch when the desired set point is reached. To further increase uniformity, the voltage applied to the sample is decreased as the z position gets closer to the desired depth. This decrease in voltage slows down the etch rate towards the end of the process so that it terminates closer to the actual set point.

All of the distance parameters in the LabVIEW program are expressed in voltages which are applied to piezoelectric actuators. When high voltages are applied across these actuators the piezoelectric material changes width. Voltages 15 times larger than those inputed on the front panel will be added to the voltages already applied to the x, y, or z piezo-electric scanner. Since positioning of the sample with respect to the tip can also be done using the included software, it is important to realize that the total voltage applied to the piezo-electric scanner is the sum of the voltage from both the internal and external source. The maximum voltage that can be applied to the piezo stacks is ±150 V. So if no voltage is applied internally the voltages in the LabVIEW program can be no larger than ±10 V. Relating these voltages to actual distances is not as straightforward as expected. If the piezo-stacks were completely linear then the conversion between voltage and distance could be easily calculated. These theoretical values are 1 mV = 1.33 nm in the x and y directions and 1 mV = 0.45 nm in the z direction. The z direction piezo has a smaller maximum travel, 4.47 µm, than the x and y direction piezos. This smaller range is traded for greater accuracy and smaller absolute displacements. For this reason the conversion factor differs from the x and y piezo stacks which each have a maximum range of 26.7 µm. The piezo stacks have non-linearities in them and so the actual relationships

between the voltage and displacement vary and are represented in Figure 3.5.

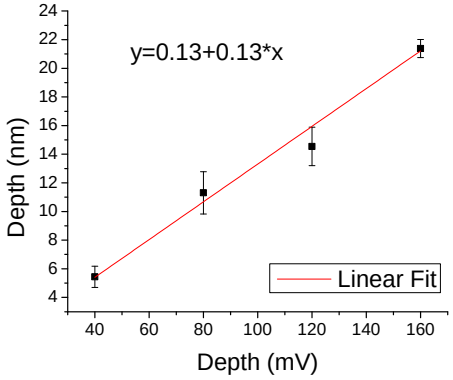

(a) The actual measured depth in nm as a function of the piezo voltage change in mV

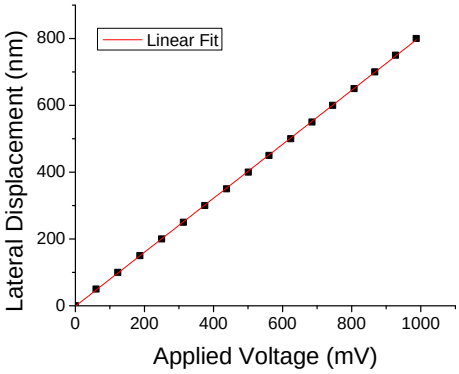

(b) The measured displacement in nm as a function of the x and y piezo voltage change in mV

Figure 3.5: Relating actual distances in the x, y, and z directions measured in nm to the change in piezo voltage applied to the respective piezo stacks.

Voltages are measured and applied between the AFM system and the LabVIEW program by means of a National Instruments Data Acquisition board (NI-DAQ). The z-axis PZT voltage is monitored by LabVIEW in order to determine when the depth set point has been reached. The x and y piezo voltages are controlled by the LabVIEW program in order to move the tip in the x-y plane for the fabrication of arrays and trenches. The bias voltage is also controlled by the program but because NI-DAQs are limited to a maximum voltage of 10 V, the voltage from the DAQ is doubled, using a voltage doubling circuit,before being applied to the sample. This allows for a maximum voltage of 20 V. Generally etching is done between 7 and 14 V.

The LabVIEW front panel displays data during the etching process and records data following each batch. During fabrication the front panel displays the number of features fabricated, the total number to be fabricated, the ini-

tial z position of the current feature, the depth set point, and several timers. Data is saved as two text files, one containing the etch times of each feature and the other the z position as a function of time for each individual etch. The file numbers associated with these text files are incremented automatically by the program.

3.1 Fabrication

All of the structures we make in HOPG are fabricated in contact mode and are defined by pixel coordinates and etch depths. The simplest structure is a pit or hole which consists of a single pixel and a particular etch depth. In addition to the pixel coordinates and etch depth, many other parameters are used to fabricate HOPG structures. These settings can be broken down into three types: displacement voltages, applied bias voltages, and measures for combating hysteresis. The first two types will be treated as they are used in the fabrication of the various structures. The third type will be treated in Section 3.1.4.

3.1.1 Holes

Holes are fabricated by entering one 0 in the Hole Positions array found on the labview front panel (See Figure B.1) and entering the desired cut depth. As long as the x and y array numbers are both set to 1 this will create a single hole. The hole will be located wherever the tip was when the fabrication was initiated. The actual depth of the hole can be estimated by using the linear fit equation in figure 3.5(a). There are several bias voltage parameters that can be

used to control hole fabrication: max bias, min bias, fraction of etch to min bias and Vbias extra. All of these can be varied at any point during the fabrication process. The *maximum bias* is the initial voltage and the *minimum bias* is the final voltage applied to the sample. These two voltages also define the range of voltages that is applied to the sample over the course of the etch. The *fraction of etch to min bias* is the fraction of the total etch depth at which the minimum voltage will be applied for the duration of the etch. *Vbias extra* is only included as a convenient way of increasing the maximum and minimum voltages at the same time during fabrication. This voltage should be set to zero at the beginning of the fabrication and used to adjust the etch rate so it remains constant.

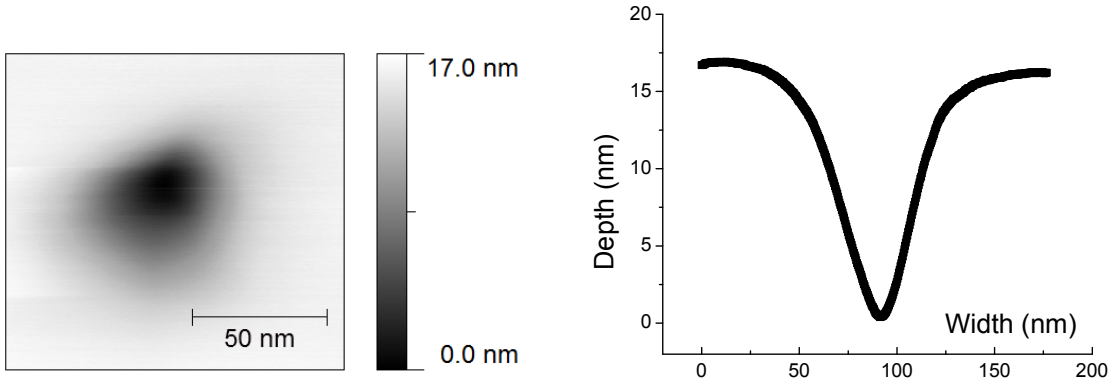

(a) Topographic AFM scan of a single hole etched in HOPG

(b) Profile of the hole in figure 3.6(a)

Figure 3.6: Hole etched in HOPG

3.1.2 Trenches

A trench is a series of overlapping holes made to a common depth. The length of a trench is determined, in part, by its depth, the pixel conversion setting, and most predominantly by the number of pixels. Deeper trenches will be longer

because the width of the holes are coupled to their depth (see figure 3.7). To a certain extent trenches can be lengthened or shortened by adjusting the spacing between the holes. However, if the spacing is too large the holes will no longer overlap and a trench is not formed. On the other hand, if the spacing is too small then the trench becomes one giant hole. The best way to adjust trench length is by increasing or decreasing the number of holes that make up the trench.

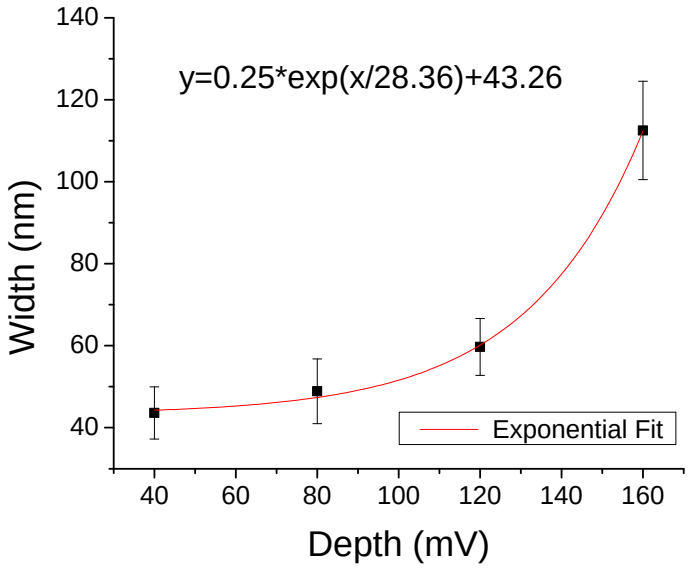

Figure 3.7: The relationship between changes in the voltage applied to the z piezo during etching and the width of the resulting hole is illustrated.

The number of pixel locations entered into the Hole Positions array will be the number of holes used to form the trench. The spacing between each of these holes is defined using the Pixel Conversion setting. This voltage can be converted to an actual spacing using .The holes are fabricated in the order in which they are listed. To fabricate a trench N pixels long, the pixels should be listed in the Hole Positions array as follows $\{0, N-1, 1, ..., N-2\}$. Endpoints are listed first, followed by the intermediate pixels starting with the second one. When

the endpoint holes are etched first, a more consistent length and a more uniform depth are achieved. The length is more consistent this way because the width of each hole is a function of the depth (see figure 3.7). Since the holes are overlapping, if they were etched in sequential order the same depth would not be etched at each point. Because the *change* in height is what is controlled not the absolute depth, the trench would get deeper with each successive hole. The overlap of the holes would result in each etch beginning slightly deeper and then etching down from that point the same distance as the previous hole. However, if the endpoints are etched first and a slope between the z positions at the bottoms of each endpoint hole is calculated. The slope is used to determine the depth setpoints for each of the intermediate holes to ensure a uniform depth regardless of sample tilt. This method also increases the consistency of the trench length.

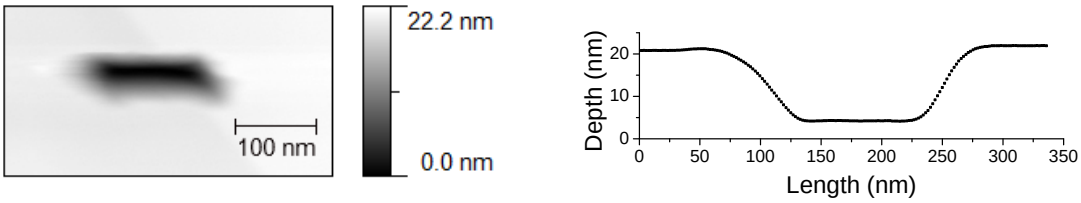

(a) Topographic scan of a single trench using AFM

(b) Profile of the length of the trench in figure 3.8(a)

Figure 3.8: Trench etched in HOPG

3.1.3 Arrays

Arrays of holes or trenches can be fabricated automatically using the LabVIEW program. The array x and array y num variables set the number of features that will be fabricated in each direction. The Array x and Array y Separation

voltages define the distance, in voltage, between the beginning of one feature and the beginning of the next feature along the respective axis. All of the same settings for holes and trenches are available in array fabrication. When making arrays of trenches two different trench lengths can be entered. The program will display the total number of features being attempted and the current feature being etched in real time.

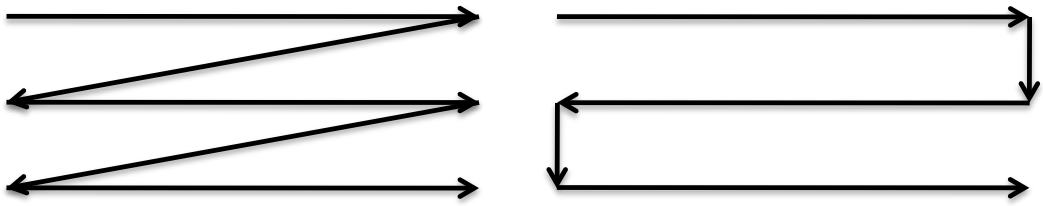

(a) Proper sequence for fabricating rows of features etched in HOPG

(b) Improper sequence for fabricating rows of features etched in HOPG

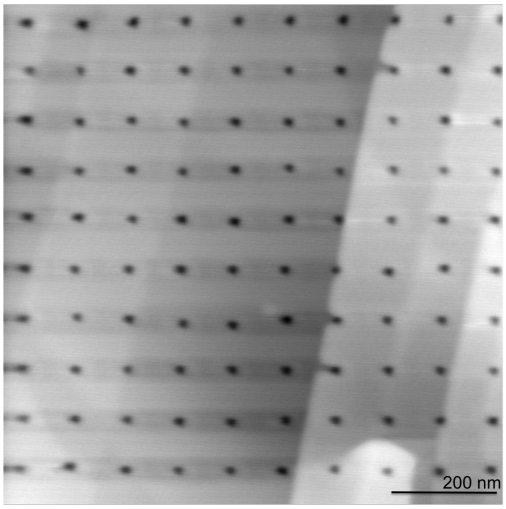

(c) Results of Proper Technique

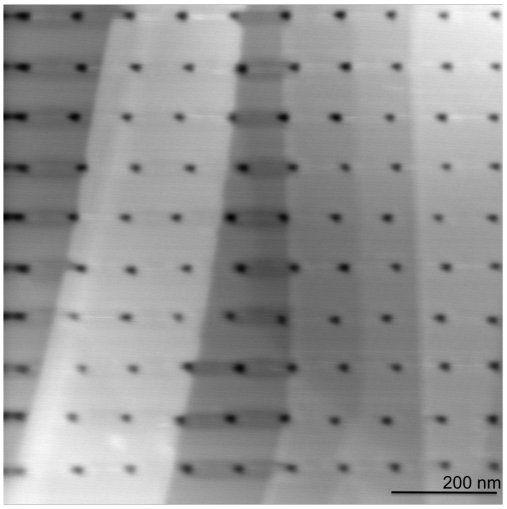

(d) Results of Improper Technique

Figure 3.9: A comparison between a raster scanning technique and a non-rastered scanning technique for etching multiple rows of features.

3.1.4 Hysteresis

There a number of settings in the program designed to decrease the unwanted effects of hysteresis. Hysteresis is a common problem which plagues all open-loop systems which utilize piezo-electric scanners. There are three methods implemented in the program to minimize hysteresis: non-rastered scanning, pauses and backlashes. The program is automatically configured to scan in a non-rastered fashion. This greatly reduces hysteresis as illustrated in Figure 3.9. The pause simply stops the program execution for a certain amount of time this allows the tip time to settle. The backlash moves the tip in both the negative x and negative y directions the amount specified and then the tip is returned. This removes accumulated charge from the piezo stack. Note, the farther the piezo has traveled in one direction the more exaggerated the effects of hysteresis are. For this reason the New Row pause and New Row backlash variables have the largest effect. (New Row refers to the after a full row is completed and the tip has been returned to a position directly below the first fabricated structure). Backlash can be also be added after each hole and each line but no benefits have been observed from doing so.

3.1.5 Tip Cleaning

Carbon deposits on the AFM as a result of the HOPG etching process. These deposits increase the tip diameter resulting in poor imaging and increased feature sizes. These deposits can be removed by applying a large, negative, sample bias– opposite in polarity from the voltages used for etching. Since etching is polarity dependent these large reverse biases do not damage the sample. In fact,

this process was used by Spinney, et al. [28] for carbon deposition onto a gold surface. No visible amount of carbon is deposited in the reverse bias because AFM images of the HOPG surface before and after cleaning the tip are identical. This cleaning process is done after each hole is fabricated. The voltage and duration can be set on the front panel of the LabVIEW program. Cleaning at $-10\,\mathrm{V}$ for $3\,\mathrm{s}$ has been shown to maintain a clean, sharp tip over several hundred etches.

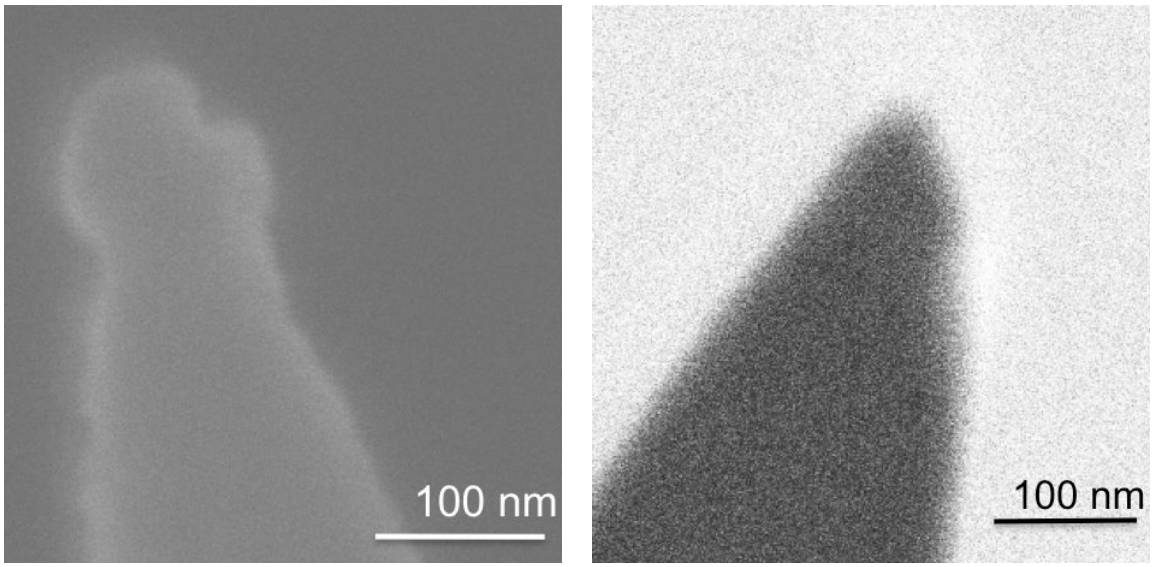

(a) SEM image of an AFM tip shows evidence of carbon deposition as a result of the etching process.

(b) SEM image of an AFM tip where a reverse bias was applied periodically during the fabrication process. No carbon deposits are visible

Figure 3.10: Reverse bias as an effective tip cleaning method

3.2 Imaging

The structures are fabricated and imaged using the same tip. Although fabrication must be done in contact mode, the surface can be imaged in either tapping or contact mode. Each option has different advantages and disadvantages. Tap-

ping mode shows finer details including a small liquid residue which is formed along the rim of the etched structures (see figure 2.4). Contact mode does not capture this residue but it produces images that are easier to use for measuring feature dimensions. The difference between these two modes should be a guide in choosing which mode to use for imaging.

3.3 Measuring

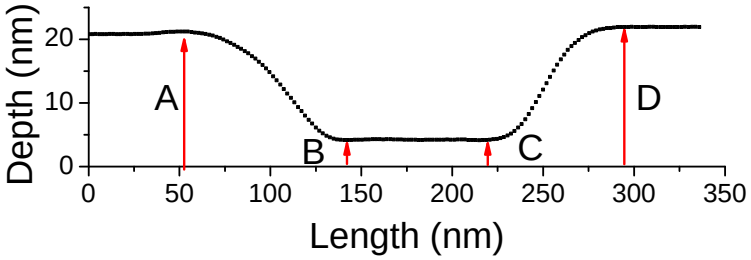

Figure 3.11: The full width at half maximum length of a trench is measured in the following way:
FWHM= x value of $(\frac{D-C}{2} + C) - x$ value of $(\frac{A-B}{2} + B)$

The dimensions of the fabricated structures can be measured using the Jeol SPM software or using Gwyddion, an open source alternative. Each of these software packages include the ability to measure depths, lengths, and widths. In measuring depth, the distance between the lowest point in the feature and the surface (avoiding the ridge formed around the perimeter) is measured on either side and averaged. Lengths and widths are both measured as Full Width Half Maximum (FWHM) values. This method for measuring the dimensions proved to be the most accurate and least biased.

CHAPTER 4

RESULTS

4.1 Holes and Arrays of Holes

Using the technique outlined in Chapter 3 an array of 100 holes was fabricated. The array is 1.5 μm^2. The pitch is 150 nm in the x and y directions. The holes have an average depth of 19.9 nm ± 2.2 nm and an average width of 32.2 nm ± 4.4 nm. The average time to etch each hole was 19.6 s ± 6.4 s.

The following parameter values were used in the fabrication of this array:

Table 4.1: Hole Fabrication Parameters

Parameter	Value
Max bias	6 V
Min bias	5 V
Cut depth	.18 V
New row backlash	720 mV
New row pause	30 s
X separation	180 mV
Y separation	180 mV

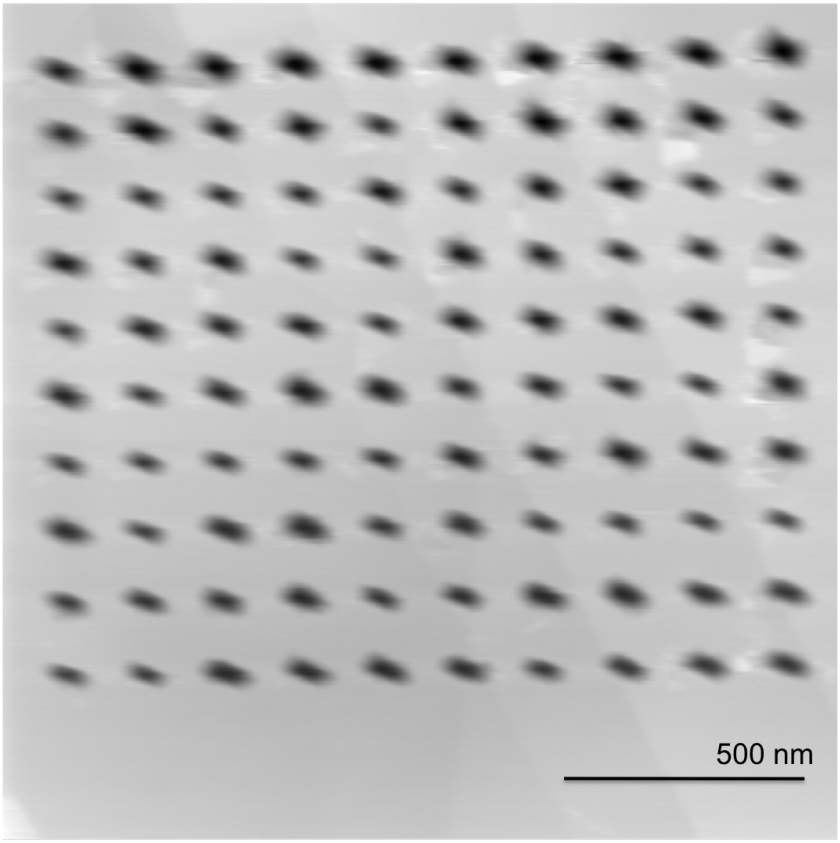

Figure 4.1: AFM topographical image showing a 10 x 10 array of holes etched in HOPG. The array is 1.5 μm^2 and the average hole depth is 19.9 nm ± 2.2 nm.

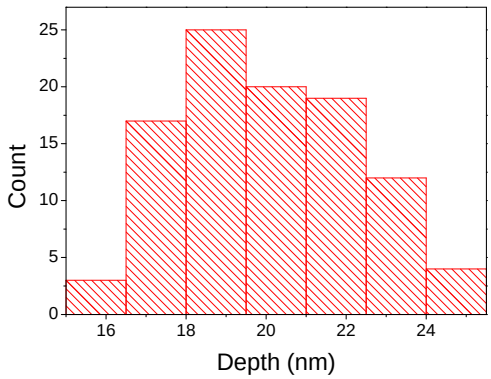

(a) Histogram showing the number of holes within a certain range of depths. Each of these holes was fabricated by applying

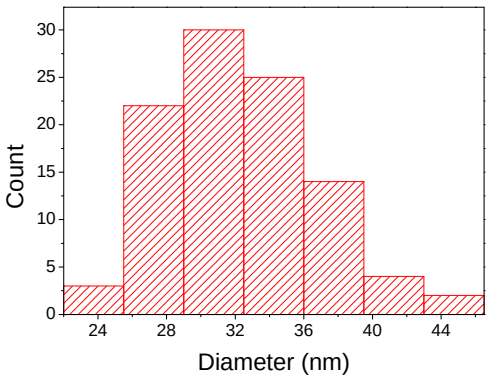

(b) Histogram of hole FWHM diameters

Figure 4.2: Distributions of hole depths and diameters

4.2 Trenches and Arrays of Trenches

Using the technique outlined in Chapter 3 an array of 105 trenches with two different lengths was fabricated. The array is 3.2 µm across and 2.2 µm down. The pitch in the x direction is 350 nm and in the y direction is 155 nm. The two lengths present in the array have an average value of 136 nm for the short lines and 183 nm for the long lines with a variation of 4.4% and 2.7% respectively. The time to etch the 136 nm lines was 38.1 s per line and for the 183 nm lines the etch time was 47.4 s per line. Included in this time is a 3 second pause between each hole.

Table 4.2: Trench Fabrication Parameters

Parameter	Value
Max bias	11.5 V
Min bias	10.5 V
Cut depth	.16 V
Pixel Conversion	.055 V
New row backlash	720 mV
New row pause	30 s
X separation	180 mV
Y separation	180 mV

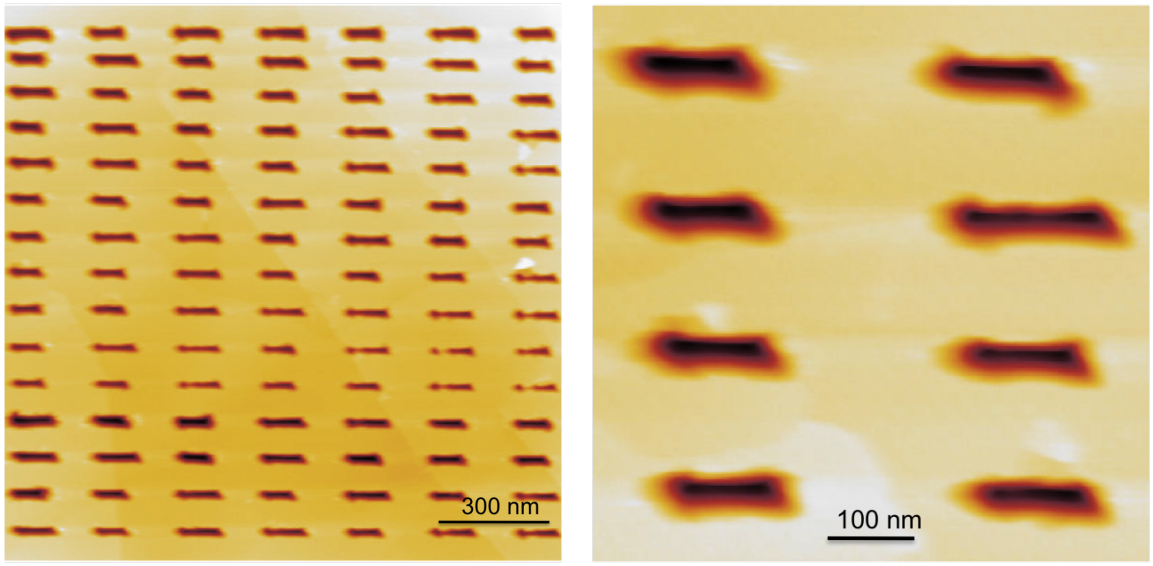

(a) Array of trenches (b) Section of array

Figure 4.3: AFM topographical images showing 105 features arranged in a 7x15 array. Two different trench sizes were randomly chosen prior to the fabrication of each trench. The first trench size was 3 holes long and the second trench size was 4 holes long. The average length for the first trench was 136 nm ± 6 nm and the average length for the second trench was 183 nm ± 5 nm

.

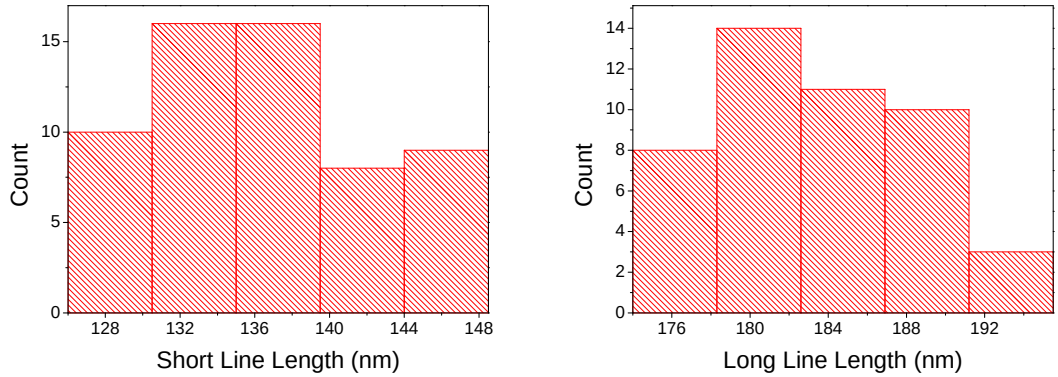

(a) Histogram showing the distribution of the 3-hole trench lengths.

(b) Histogram showing the distribution of the 4-hole trench lengths.

Figure 4.4: Distributions of lengths for short and long lines.

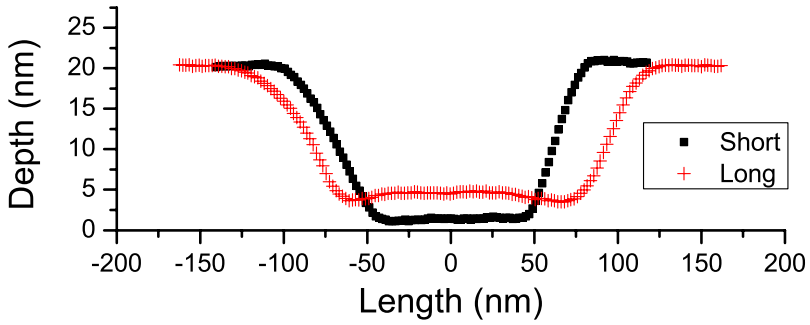

Figure 4.5: Profile showing the length and depth of a typical short and long line.

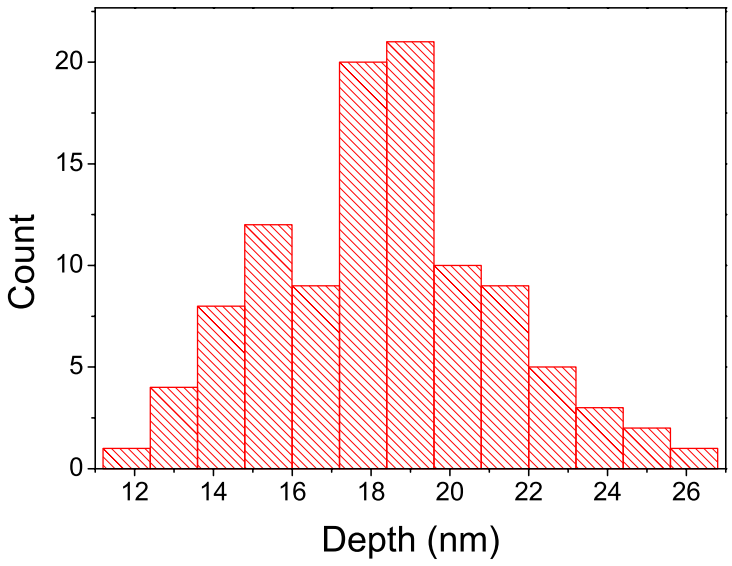

Figure 4.6: Distribution of depths for etched lines

Consistently placing features precisely relative to other structures is a continual struggle as a result of intrinsic properties of piezoelectric materials: nonlinearity and hysteresis. The response of the x and y piezos are not linear over their entire range. Restricting the amount of travel in x and y will keep positioning within the linear regime and thus make it more precise. The other issue, hysteresis, can be greatly reduced by always approaching the desired feature position from the same direction. This technique for reducing the effects of hysteresis is illustrated in Figure 3.9. Additional information regarding fabrication problems are addressed in Appendix A.

CHAPTER 5

DISCUSSION

5.1 Effect of Etch Rate on Feature Quality

The feature quality is directly affected by the etch rate. There is an optimum etch rate at which the highest feature quality is achieve. If the etch rate is too high it results in inconsistent dimensions and more tip damage, possibly due to more mechanical damage and deposited carbon. Etching too slowly, however, drastically increases fabrication times, and the increased time allows longer lateral drifts in tip position resulting in degraded feature quality. In addition, the graphite may undergo oxidation rather than etching as described above.

5.2 Temperature Dependence

The feature size is determined by the size of the meniscus that forms between the scanning probe tip and the HOPG surface. The meniscus size is mainly determined by environment, probe parameters, and tip height [29]. However, the feature size can be decreased by the HOPG temperature. As the temperature of the HOPG surface increases, the evaporation rate at the edges of the meniscus increases, resulting in a narrower meniscus and smaller feature size. The data is shown in Figure 5.1, where a 35^{o}C increase in HOPG temperature results in a 24% decrease in the full width half maximum of 24 nm deep holes. The Arrhenius equation predicts an increase in the etching rate as the surface temperature is elevated. Instead, the etching rate slows at higher temperatures due

to increased instability of the meniscus. The thermally-reduced meniscus yields smaller feature sizes but with increased etch times.

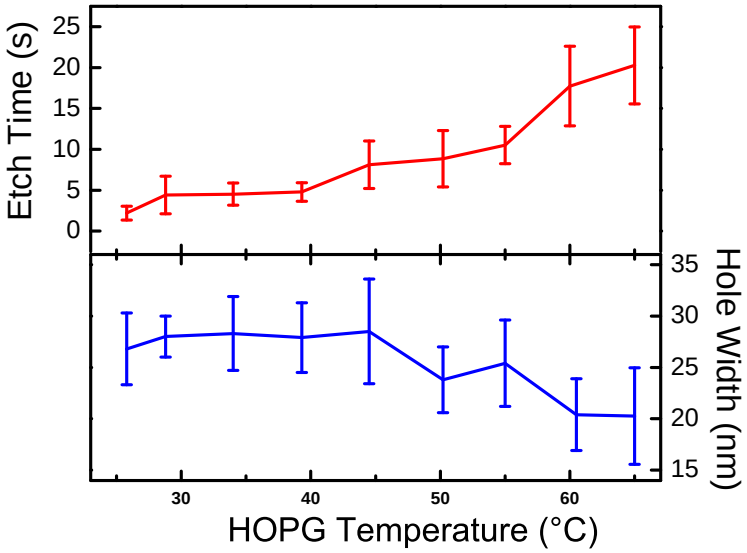

Figure 5.1: The top graph shows that the time to etch the same size feature increases with increasing temperature. This is a result of the meniscus instability at elevated temperatures. The bottom graph illustrates the decrease in feature width as the temperature increases. This shows that the decrease in meniscus radius at higher temperatures translates in to smaller features.

5.3 Conclusion

Consistent nanometer-scale fabrication techniques for carbon-based materials will aid in a variety of applications across several fields of study. AFM systems are used routinely to move nanotubes, molecules, and other small particles the ability to flexibly pattern the substrate with the same system provides a lot of power.

DNA has been shown to reliably form networks and films on HOPG surfaces. AFM systems are the predominate method for studying adsorbed DNA and can also be used for genomics and DNA sorting. One goal of the biology community is to perform nanomechanical measurements on suspended DNA. A scheme to etch away the HOPG surface releasing DNA membranes for this sort of measurement could be realized using this etching method. [30]

Carbon-based materials have also been the substrates of choice for many new biosensors. Carbon nanotubes, graphene and HOPG have all been used in the development of biosensors. This novel method provides a very flexible way to pattern these devices. [31]

Graphene and multi-layer HOPG are also good candidates for mechanical resonators because their large elasticity translates into high frequency operation. One of the challenges in this field is defining the resonators using conventional lithography techniques because consistent coverage of graphite films this thin at the wafer-scale is not currently achievable. Since masks are not used in this novel HOPG etching technique, each wafer can be patterned according to where the best film has been deposited instead of making a custom mask for each sample. [32]

Perhaps the most compelling application for this AFM-based etching process is fabricating graphene nano-ribbons (GNR). The necessary resolution for this application is not achievable yet but improvements may make this technique viable for defining GNR devices. The electronic properties of GNR's vary dramatically (semi-conducting to metallic) with the exact atomic width of the channel [33]. This feature makes atomic resolution necessary to use GNR's in any practical device. With a current minimum feature size of 1 nm this level of resolution is not out of the realm of possibility.

APPENDIX A

TROUBLESHOOTING

The methods chapter explains the basic process. The process, however, has many uncontrollable variations which makes it very difficult to simply repeat these steps. In this section these variables, the problems they cause, and possible solutions will be discussed.

A.1 No Etch Even at High Voltages

If no etching occurs at 10 V then the process is not working normally. There is no single solution that will solve this problem but there are a number of things that can be tried. First, check to make sure that the z piezo is maintaining a constant average value. Second, scan the surface then move the tip over and scan again. Make sure that features from the first scan are still present in the second scan. If they are not, then the tip is not in contact with the surface and the tip should be moved closer to the sample surface. Third, check all of the connections and make sure that nothing is disconnected.

A.2 Z Piezo Drift

After the final approach has been made in contact mode often the z piezo voltage will not remain constant. As long as the average value is constant then this is not a problem but if the piezo voltage is steadily increasing or decreasing the etching process will not work. This is can caused by charge buildup in the piezo

stack. When the tip is retracted using the "tip retract" feature on the JEOL high voltages are applied to the stack to keep the tip retracted. If the tip has been in this retracted state for a long time the piezo will take a very long time to settle sometimes multiple hours.

The best thing to do is to shut the machine completely down and come back in a few hours. This allows the excess charge to drain off the PZT. If the problem persists then try and make sure that minimal voltage is being applied to the piezo. There are two mechanisms used to approach the tip to the sample, the stepper motor and applying voltage to the z piezo stack. The stepper stage is used for course adjustments in height and the piezo stack for fine adjustments. Ideally, when the tip is approached the piezo voltage should be negative and once it is brought close to the stage using the stepper motor the piezo voltage can be increased towards zero to make contact with the sample.

A.3 X,Y Piezo Issues

There are two major issues associated with the x and y piezo stacks, linearity and hysteresis. The response of the x and y piezo stacks are not linear over their entire range. From experience, it seems that they are mainly linear within a 4 μm^2 square centered at the origin. However, even within this range there are substantial hysteresis effects. The best way to minimize these effects is to always begin from the same side when making features. The proper and improper technique are illustrated in Figure 3.9. In addition to scanning in this manner, increasing the backlash also help decrease the hysteresis effects.

A.4 Coupling of Channel Signals

The demultiplexer in the NI-DAQ is unable to handle sample rates much higher than 20 MHz. If the sample rate is higher than this, charge will accumulate and as the different channels are sampled some of the previous signal will be incorporated into the next channel. For example, consider the z piezo is being monitored on channel 1 and the bias voltage is being applied via channel 2. If the sample rate is above 20 MHz, a large amount of fluctuation can be seen in the applied bias as a result of residual charge from the z piezo voltage. This problem is easily solved by reducing the sampling rate to the proper value.

A.5 Etch Stops During Fabrication of Large Array

During the fabrication of large arrays for some reason etching will slow dramatically or even stop as the tip moves farther from the initial position. This could occur for a variety of different reasons including variations in the: tip shape and surface, tip-sample separation, environment, applied bias, etch time, and temperature. The etching generally resumes with an increase in applied bias voltage and/or moving the sample closer to the surface by changing the reference voltage.

APPENDIX B

LABVIEW PROGRAM

LabVIEW is a platform and development environment for a visual programming language from National Instruments. LabVIEW is short for Laboratory Virtual Instrumentation Engineering Workbench. Each program consists of two components the front panel which serves as the user interface and the block diagram where the program is written. This chapter includes the front panel which displays the parameters that can be set by the user and contains images of the block diagram program.

The program itself consists of 3 major loops which run in parallel. Figure B.2, the first of these loops, applies the sample bias and the x, y, and z piezo voltages. Figure B.3 reads the current z piezo position which corresponds to the current tip height. This is monitored during the etching process so that the etching can be terminated when the tip reaches a certain depth. Figure B.4 is the third and largest loop which does everything else. The rest of the block diagram figures include all the embedded loops in this third loop. Some of the figures include captions if additional explanation is needed.

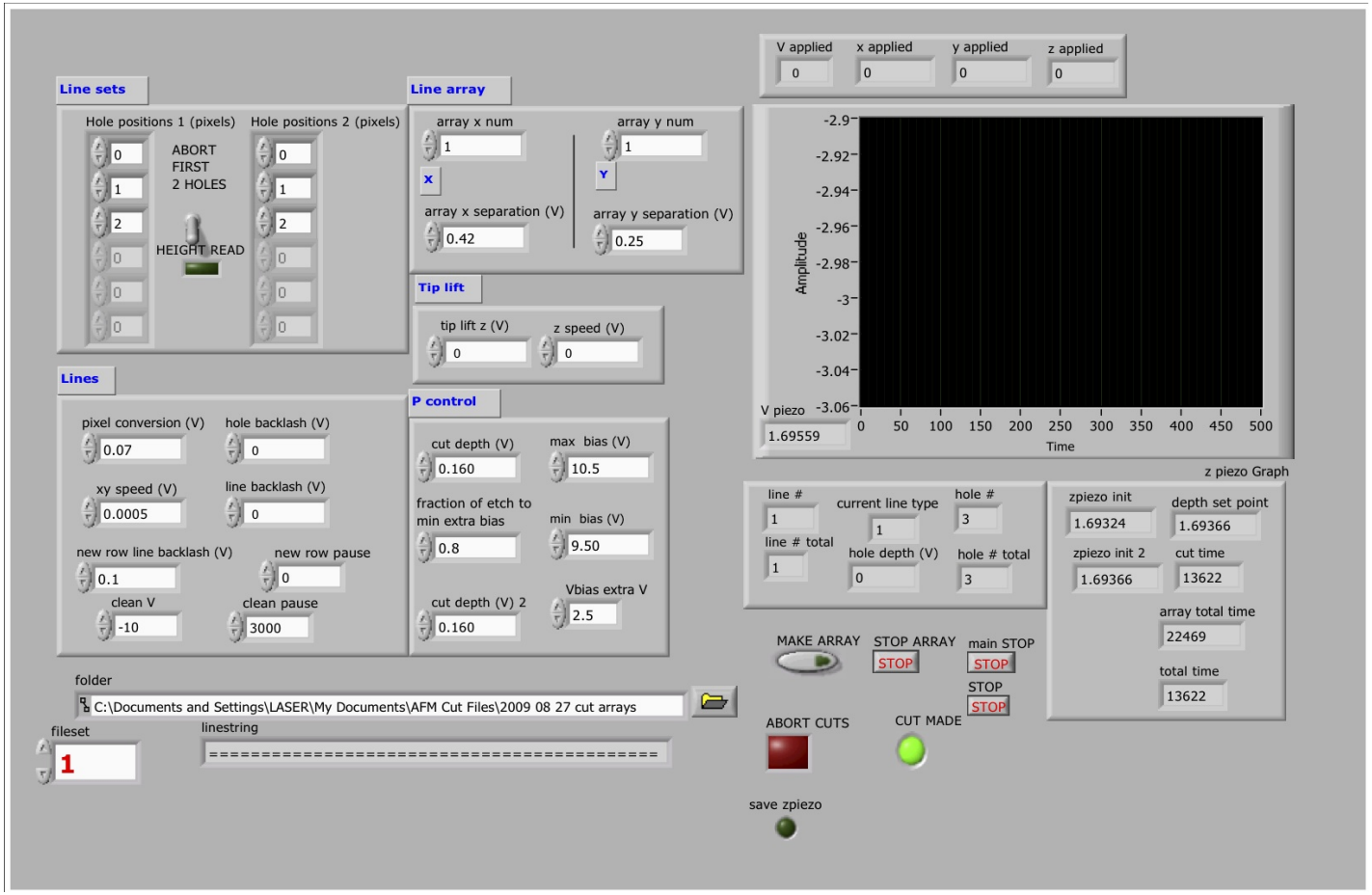

Figure B.1: LabVIEW Front Panel, the user interface used to control the etching process. All of the parameters can be set in this window.

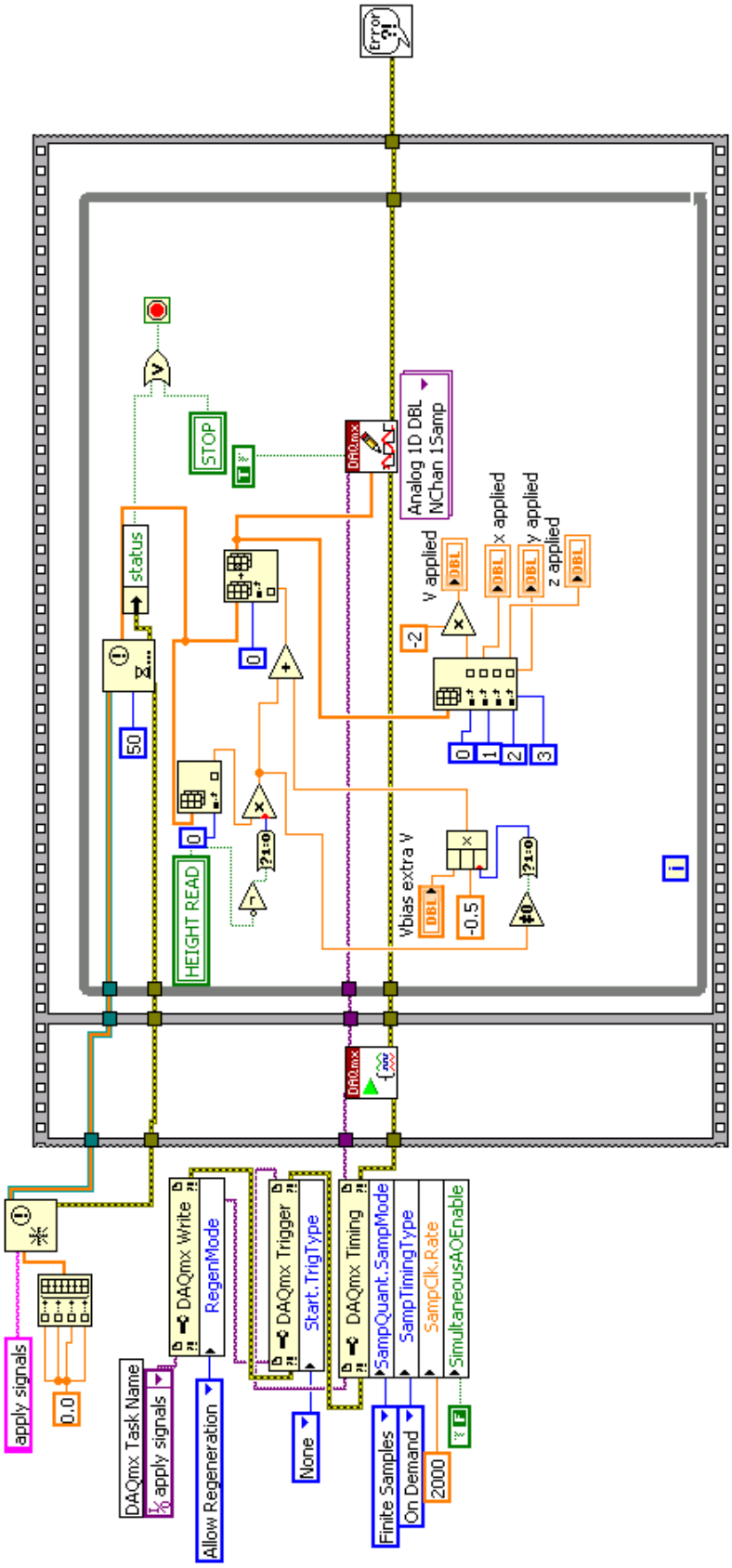

Figure B.2: Loop 1: This loop applies the bias voltage and the voltages applied to the x, y, and z piezo stacks.

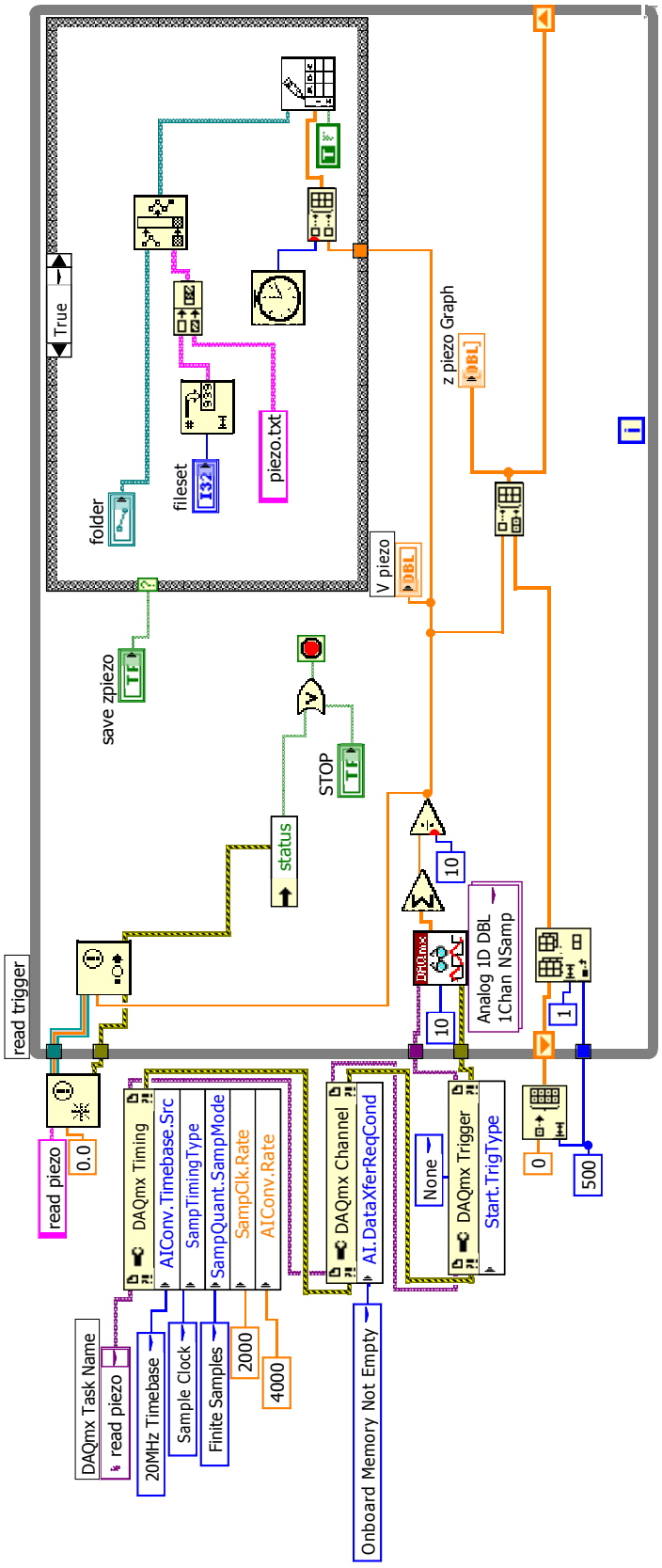

Figure B.3: Loop 2: This loop reads the z piezo voltage which indicates the current tip height and is used to monitor the depth of the etch. (The false case of the true/false loop is empty)

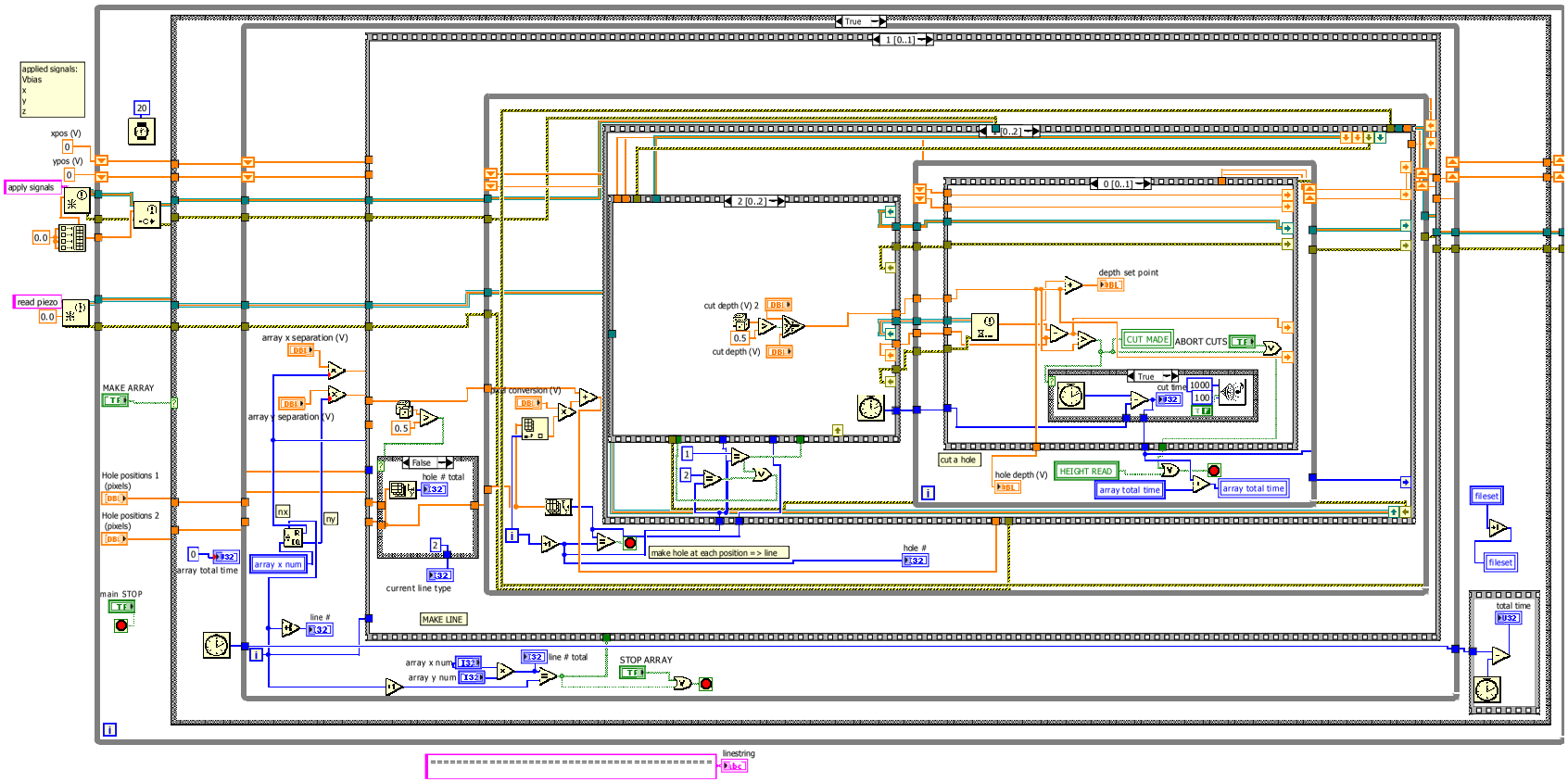

Figure B.4: Loop 3: This loop contains the rest of the program's functionality and is run in parallel to Loops 1 and 2 pictured in figures B.2 and B.3.

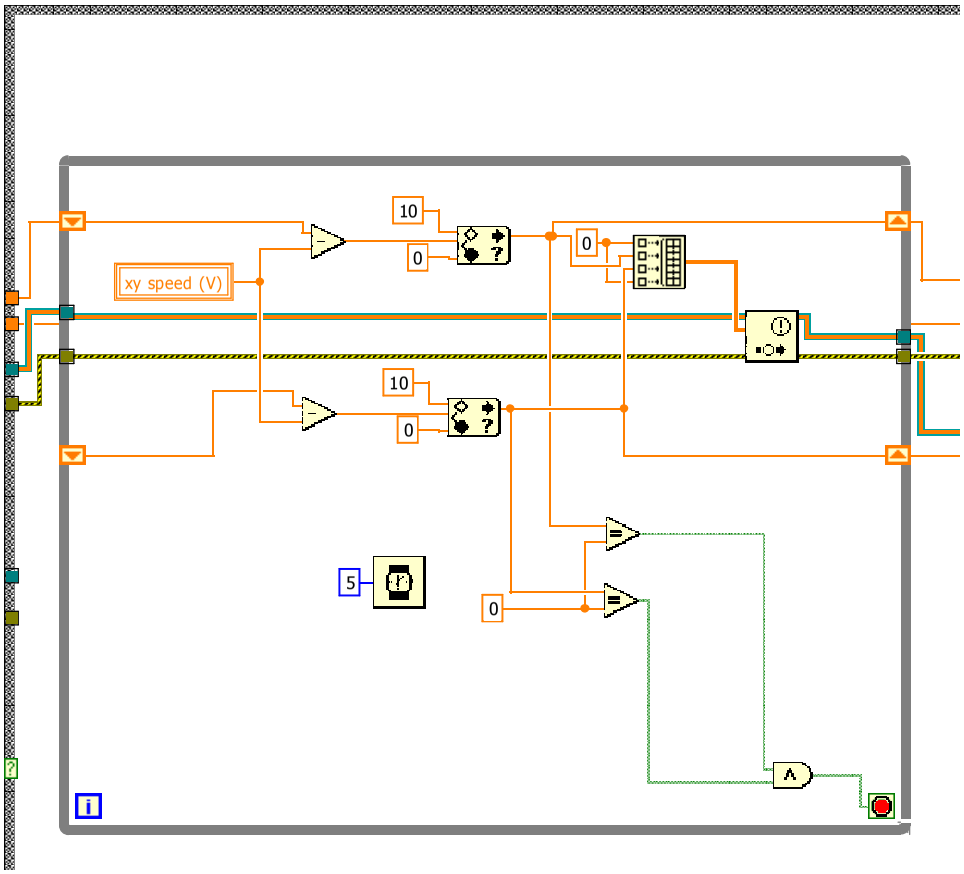

Figure B.5: This is the false case of the loop shown in figure B.4. All of the unconnected wires at the right of the page are connected to the edge of the loop. The rest of the loop is empty so that is why only a portion of it is pictured here.

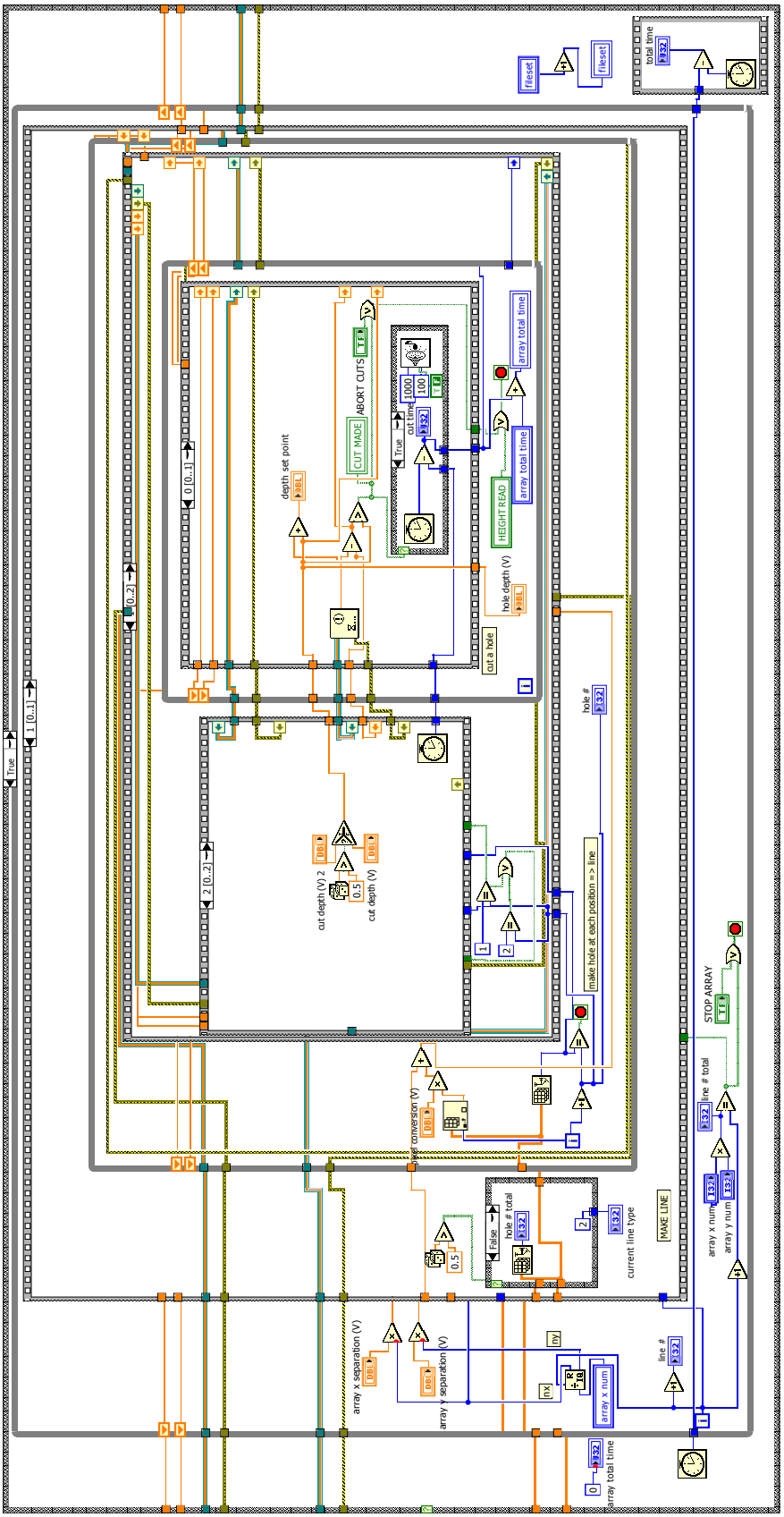

Figure B.6: This is the true case of the loop in shown in figure B.4.

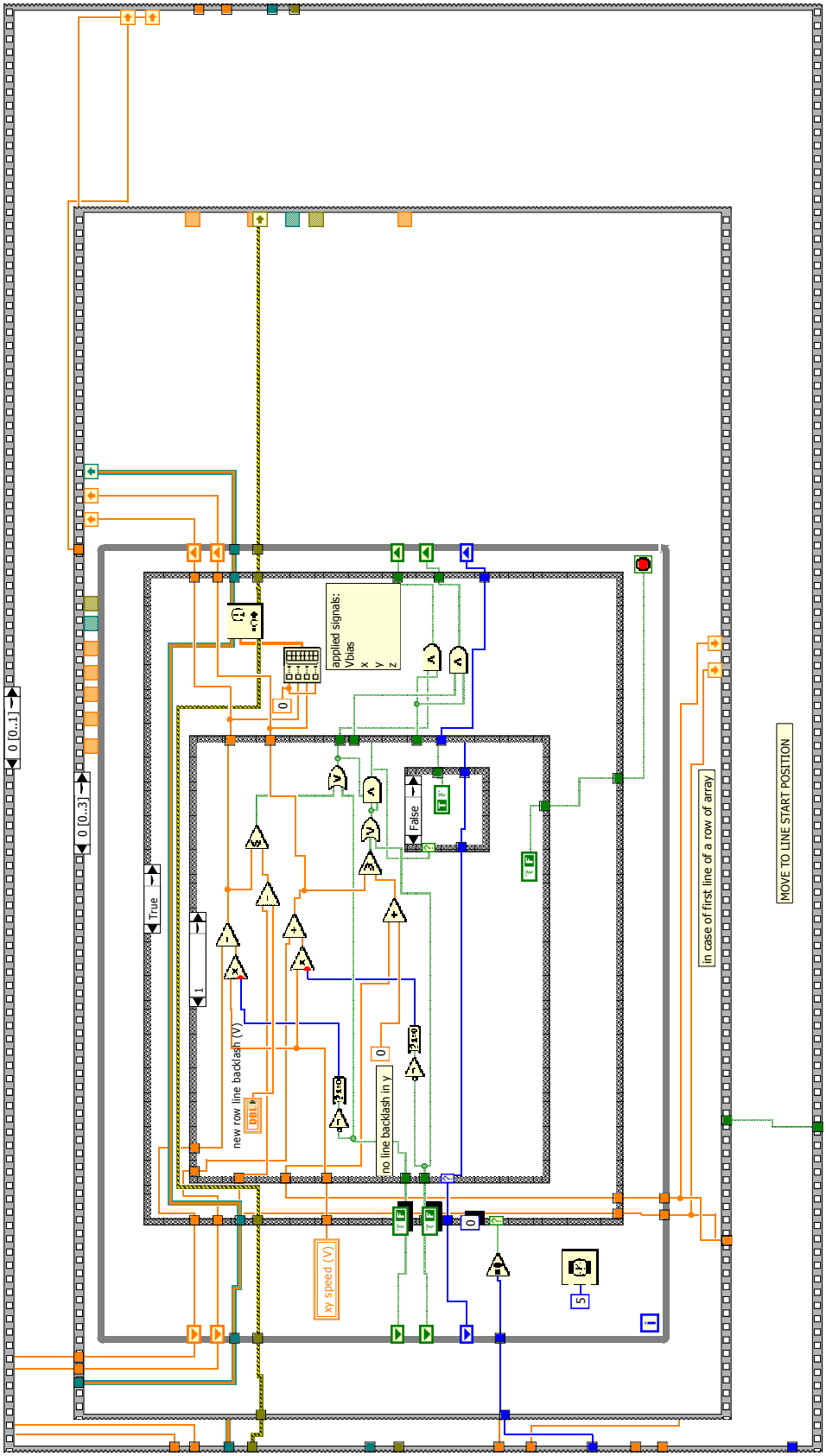

Figure B.7: This and the rest of the figures are code contained in the true case of loop 3.

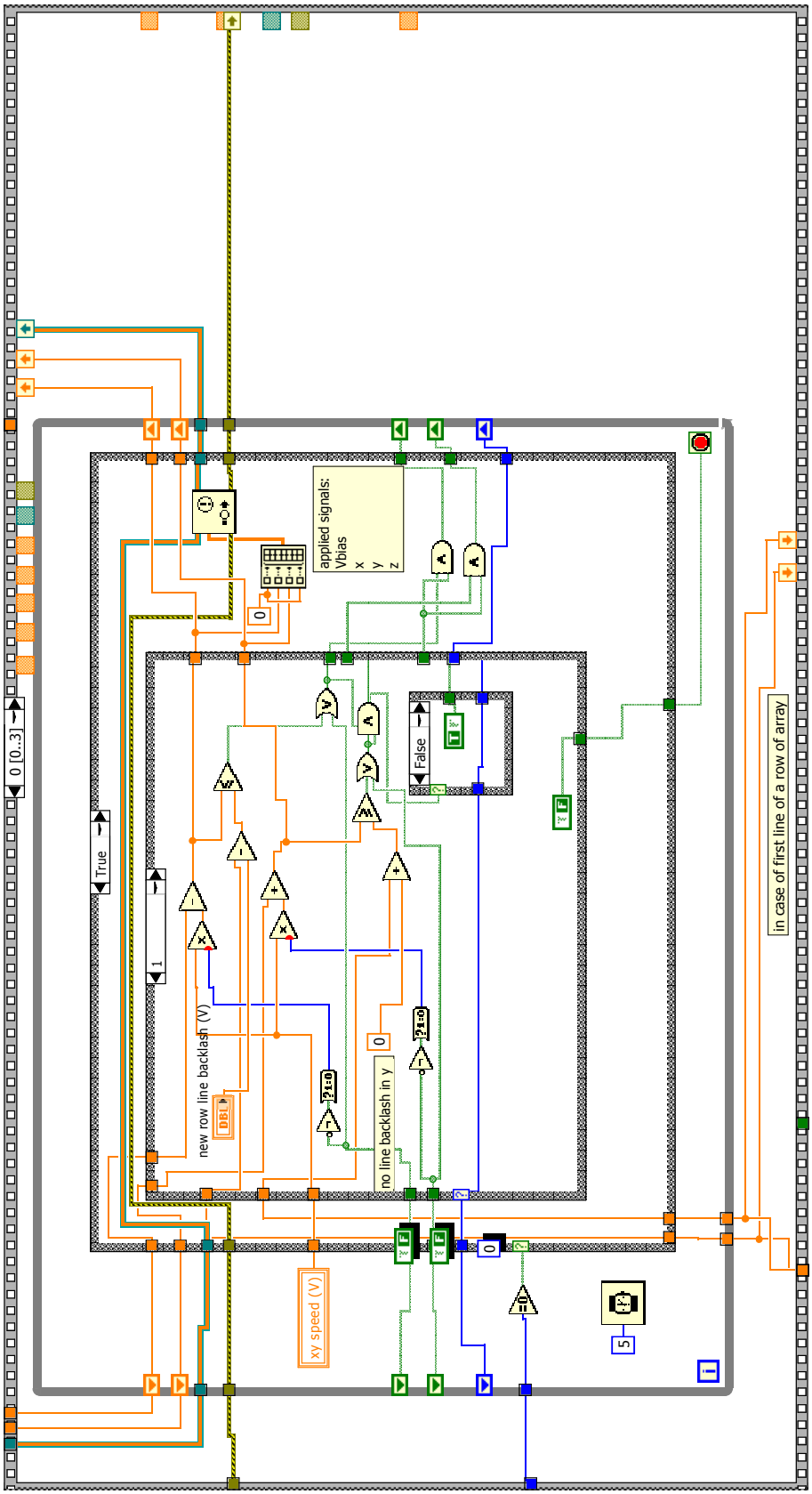
applied signals:
Vbias
x
y
z
0 [0..3]
True
False
1
new row line backlash (V)
no line backlash in y
xy speed (V)
in case of first line of a row of array
5

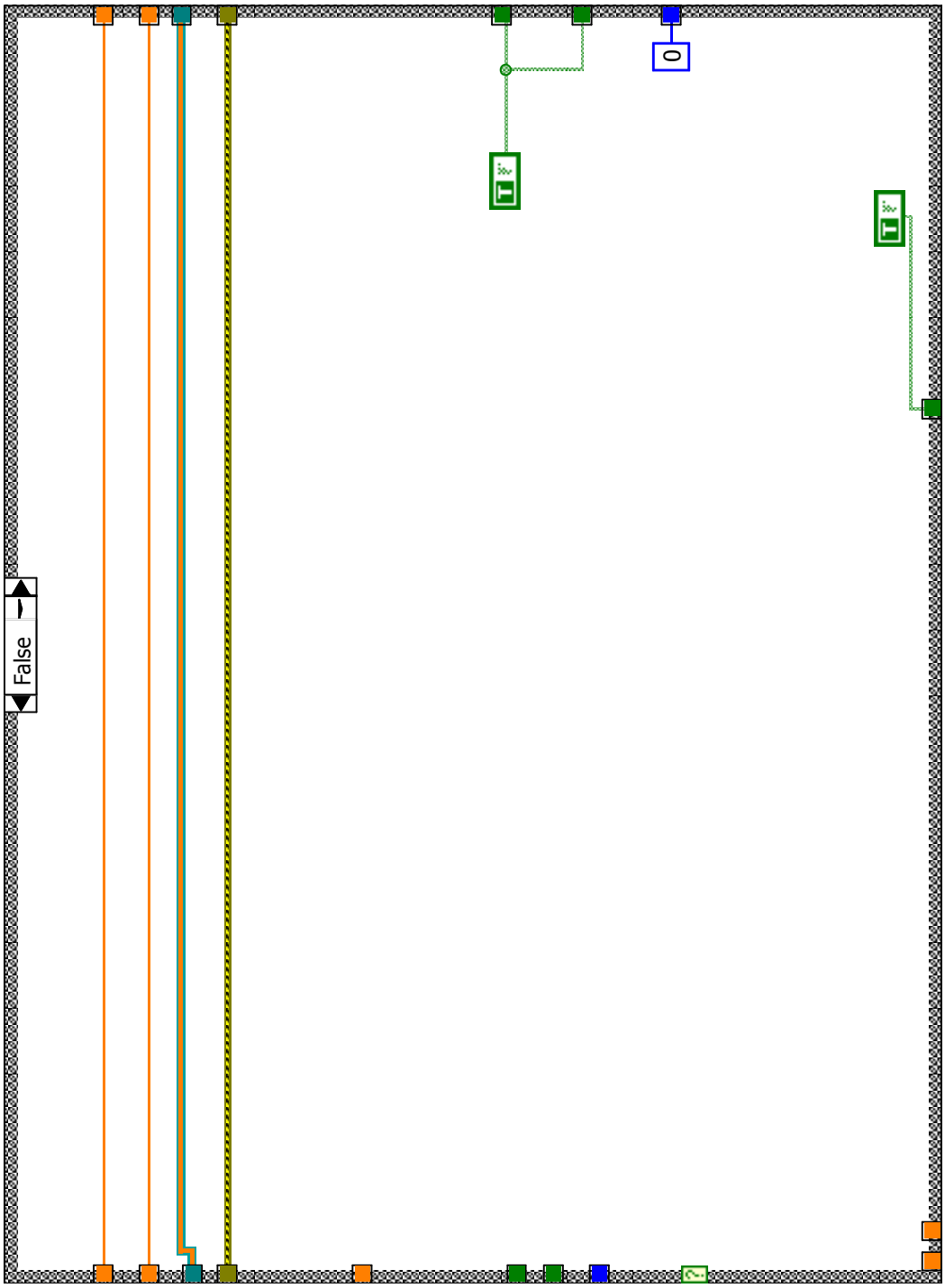
0
False

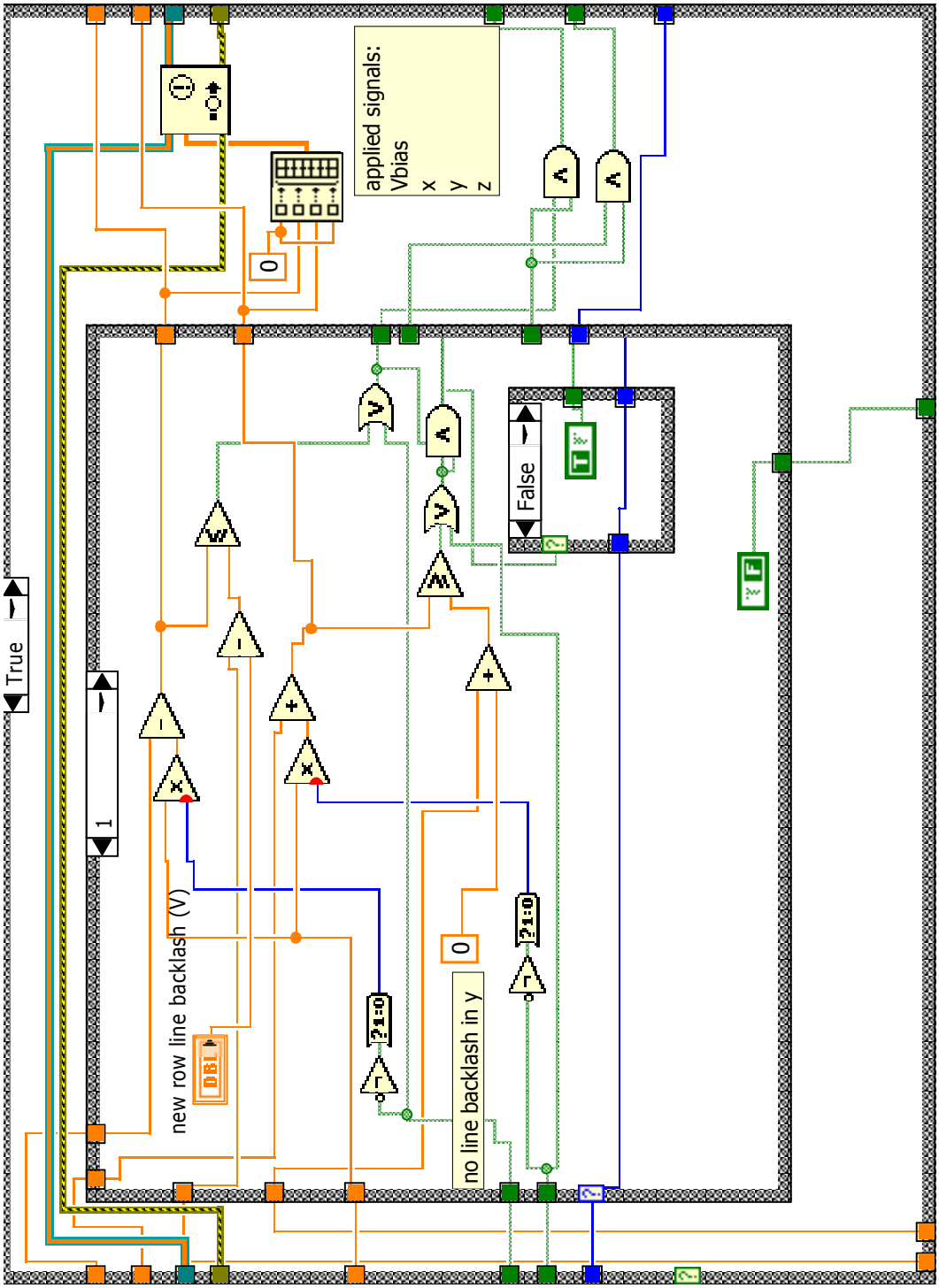
applied signals:
Vbias
x
y
z
0
True
False
1
new row line backlash (V)
no line backlash in y
0
21:0
21:0

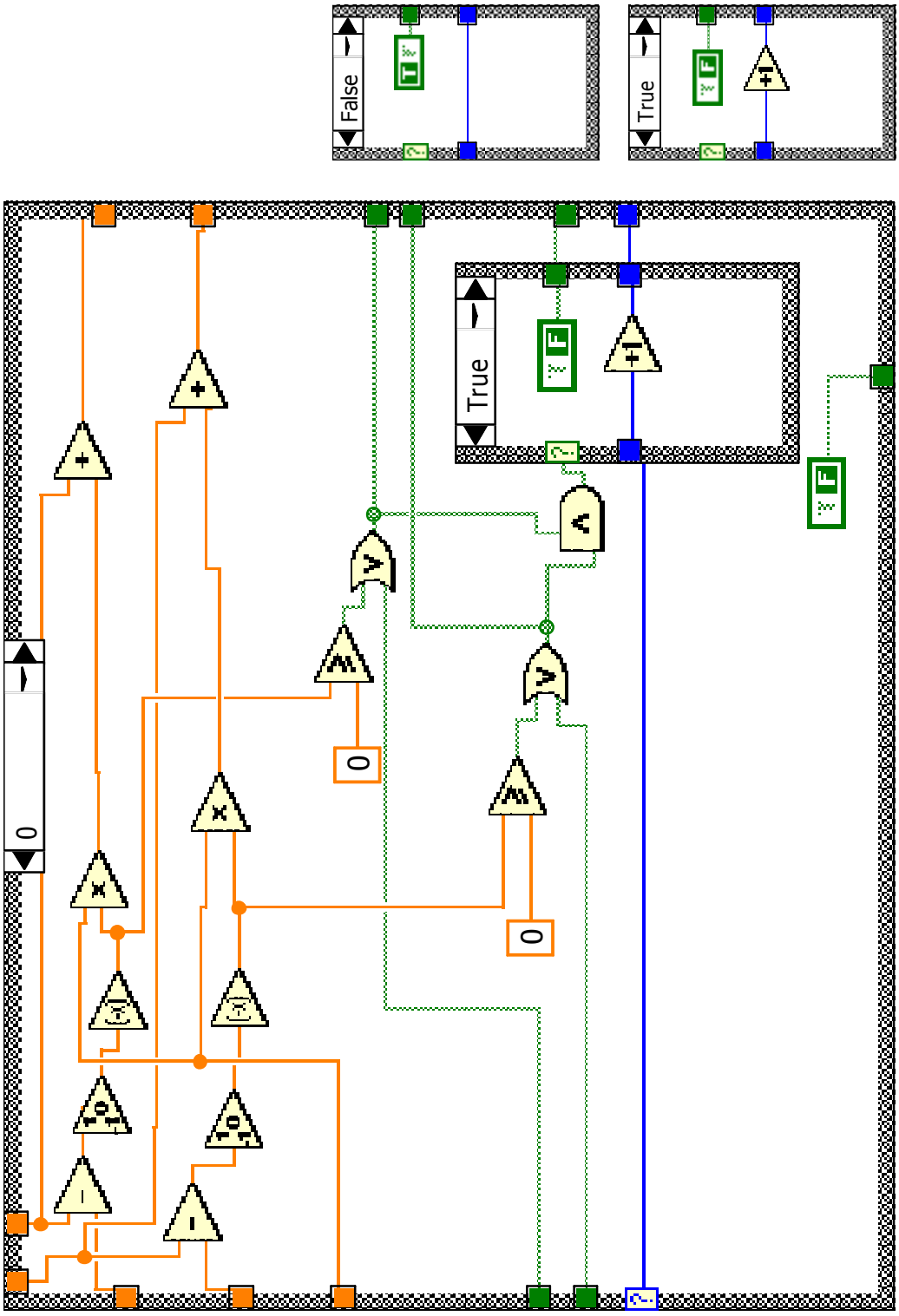
False
True
True
0
0
0

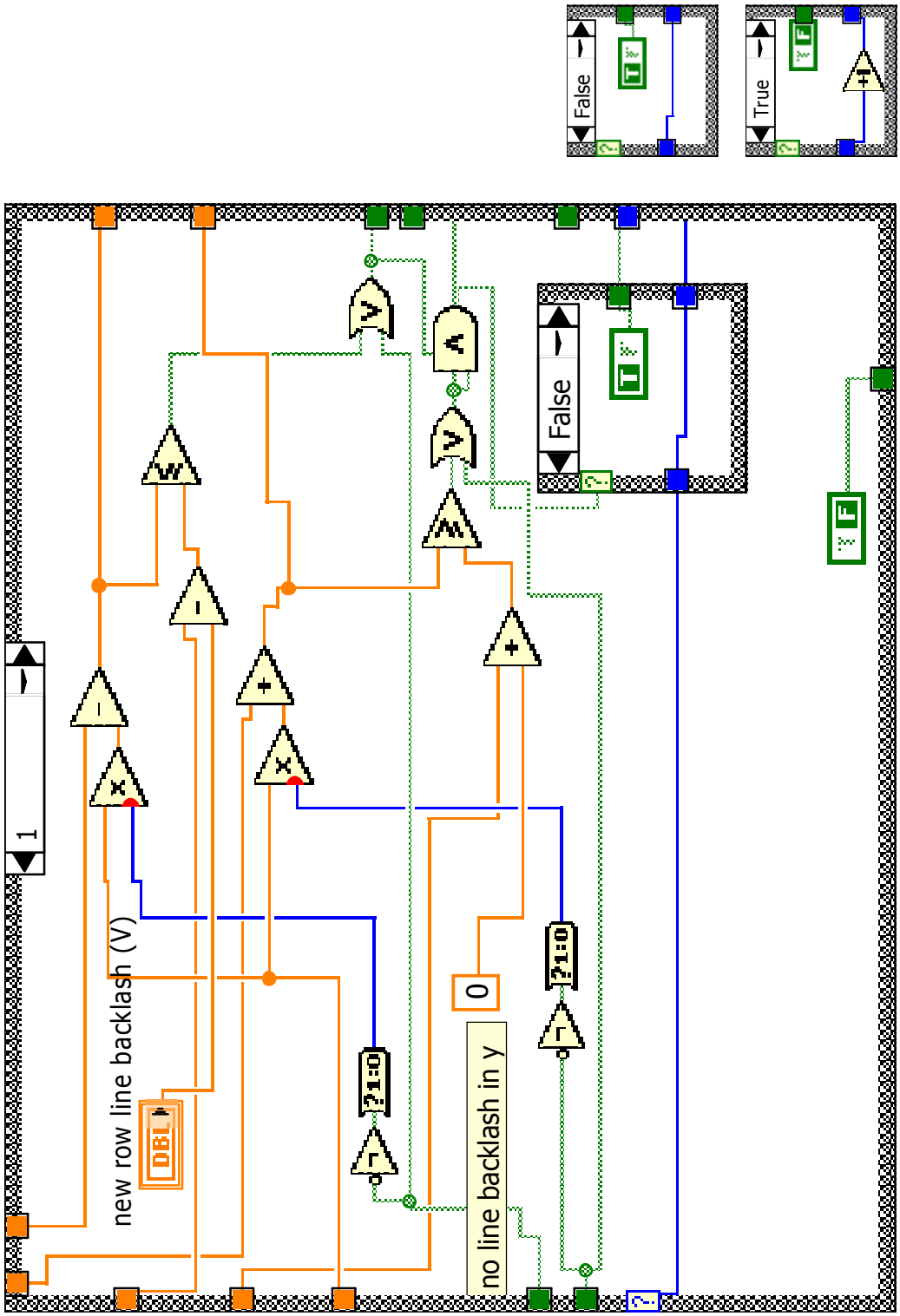
False
True
1
new row line backlash (V)
DBL
21:0
0
no line backlash in y
False

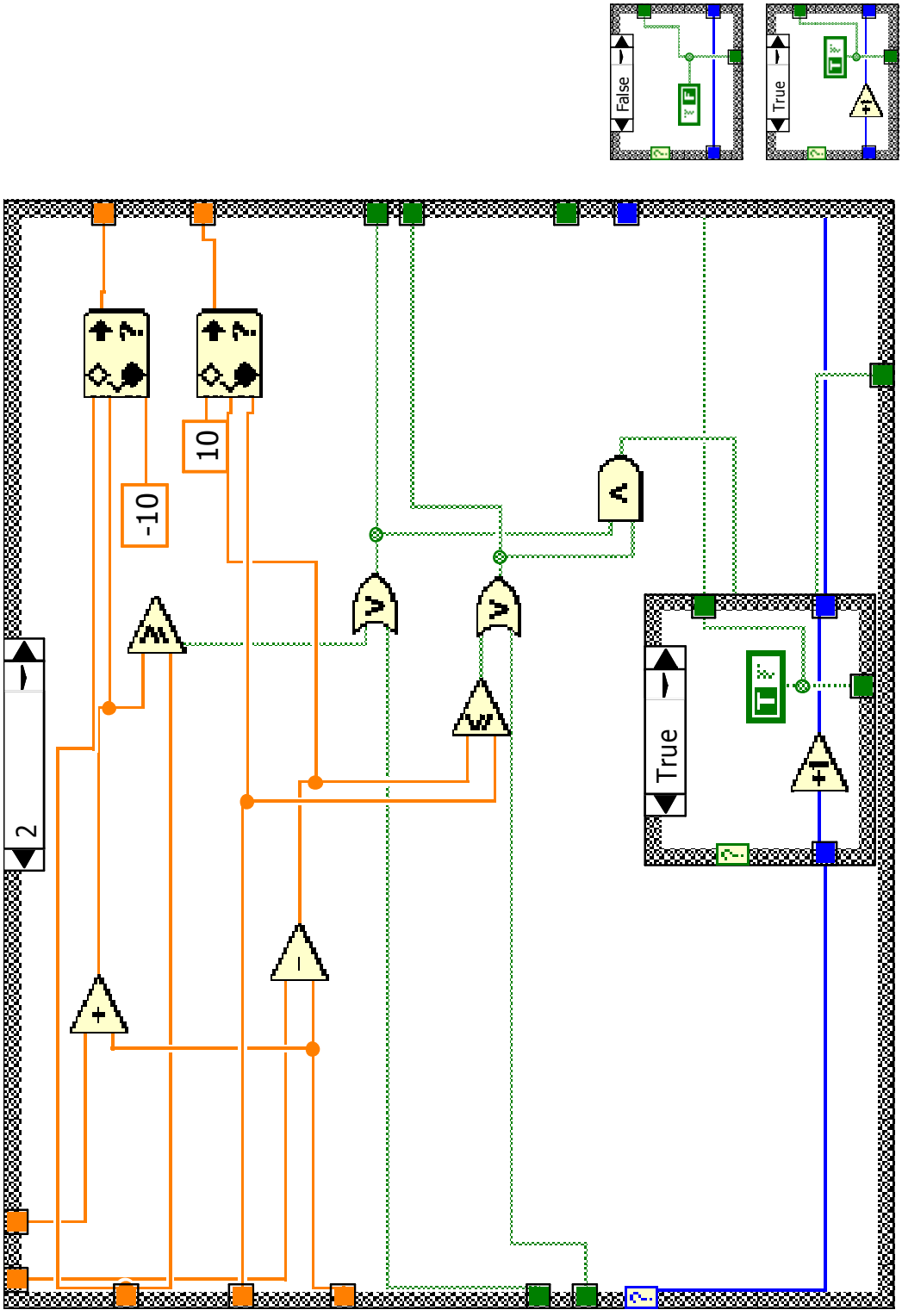
False
True
10
-10
2
True

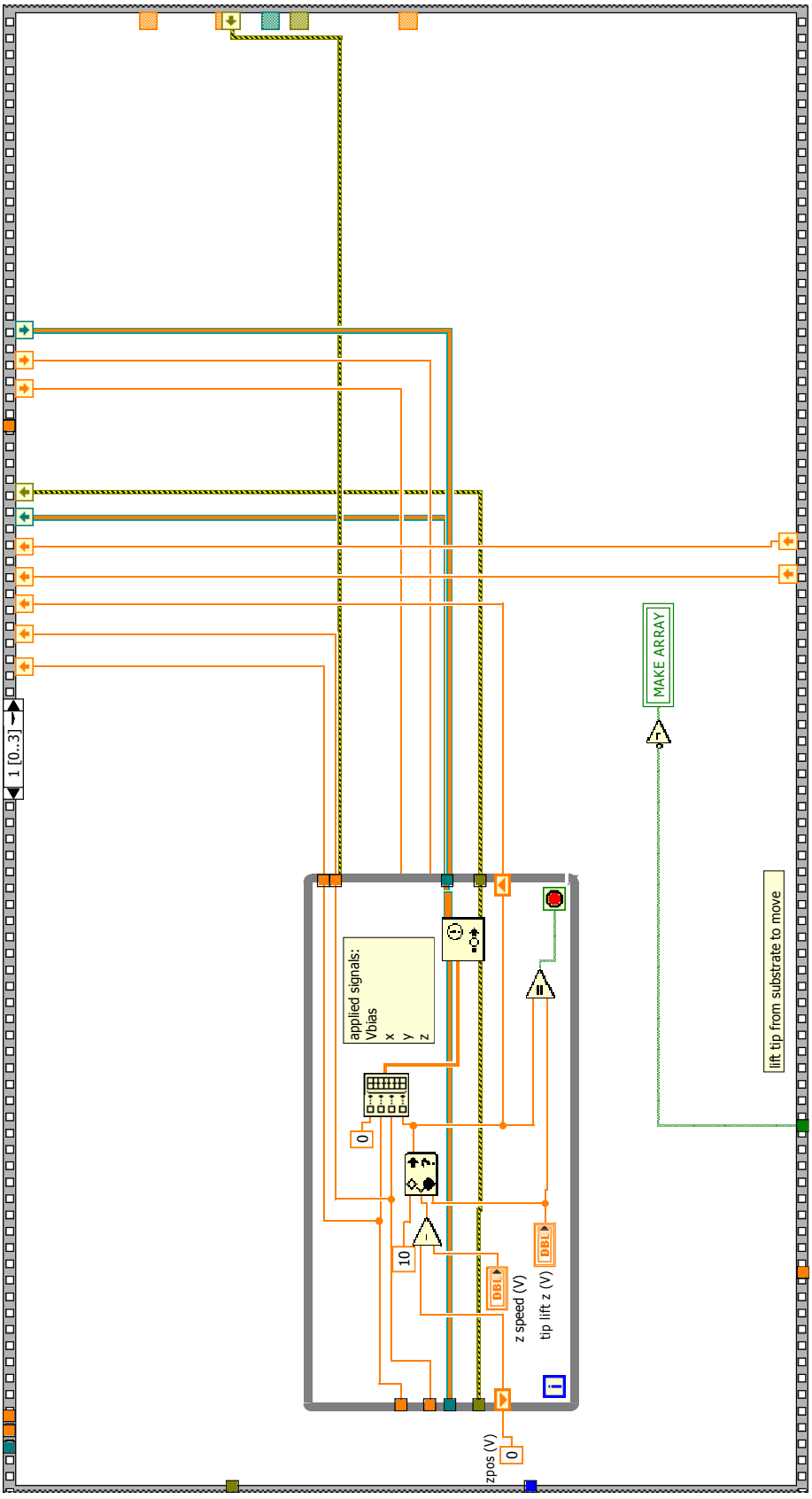
1 [0..3]
MAKE ARRAY
lift tip from substrate to move
applied signals:
Vbias
x
y
z
0
10
DBL
z speed (V)
tip lift z (V)
zpos (V)
0

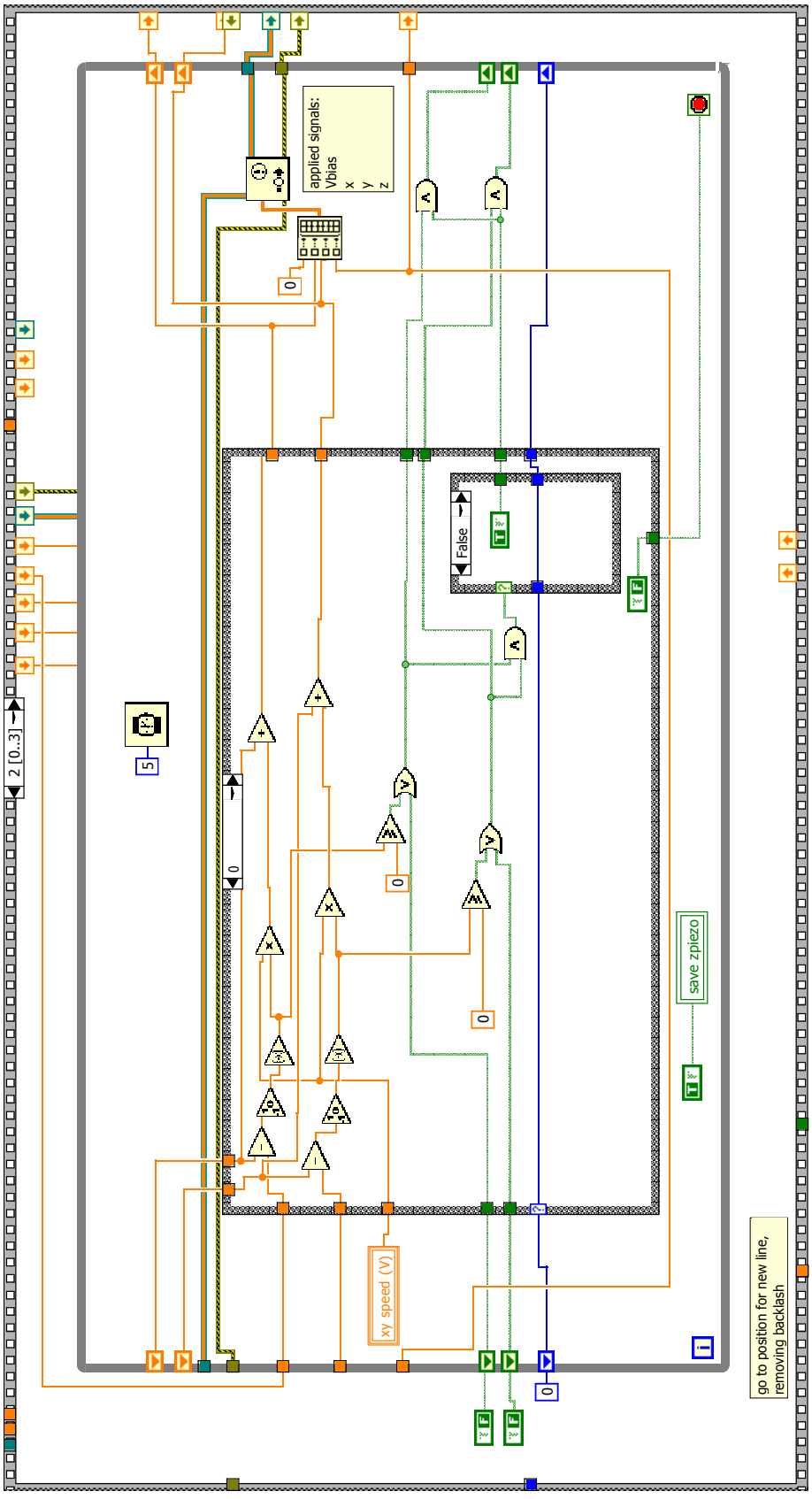
applied signals:
Vbias
x
y
z
False
2 [0..3]
5
0
save zpiezo
xy speed (V)
go to position for new line,
removing backlash

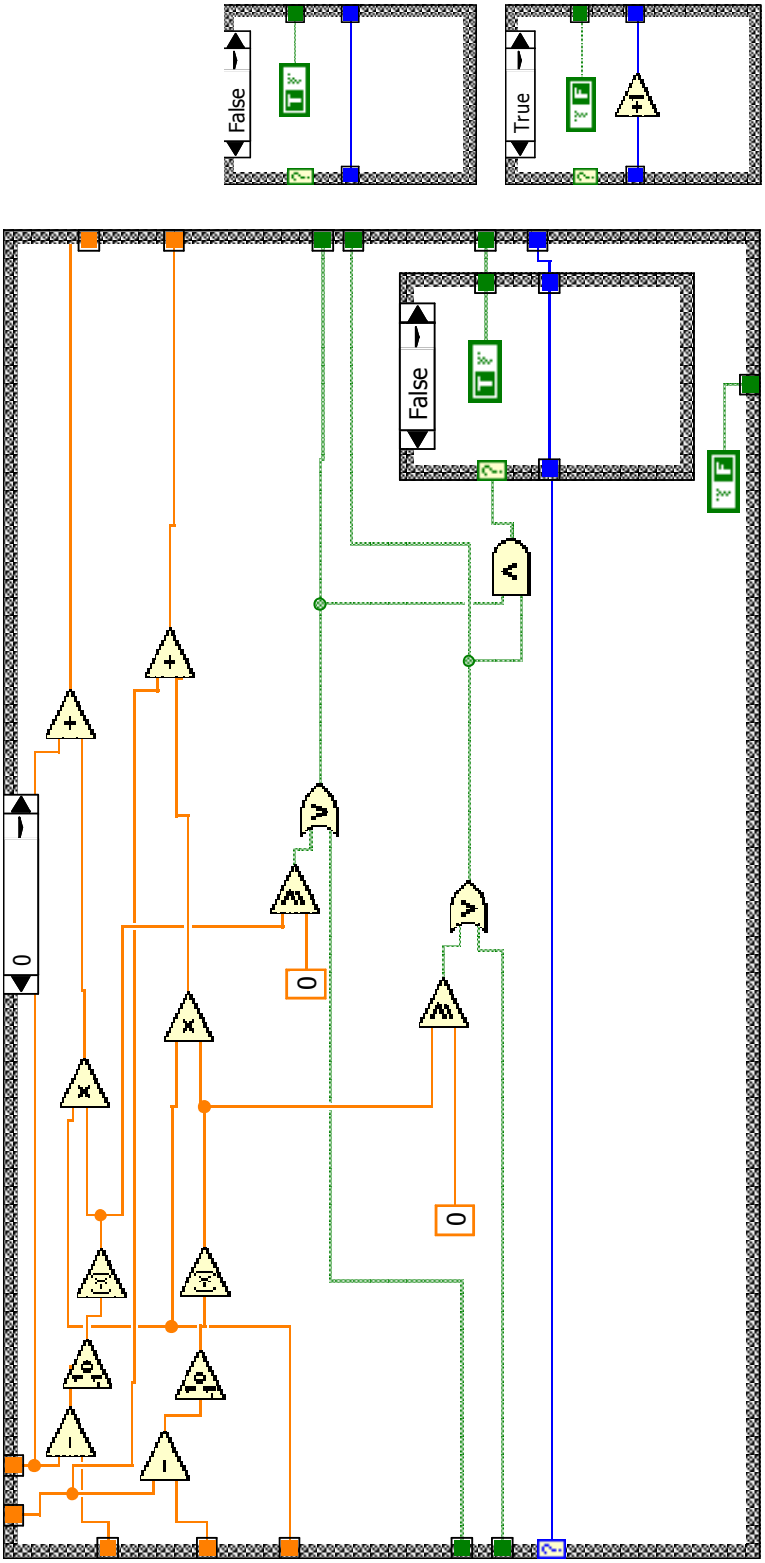
False
True
False
0
0
0

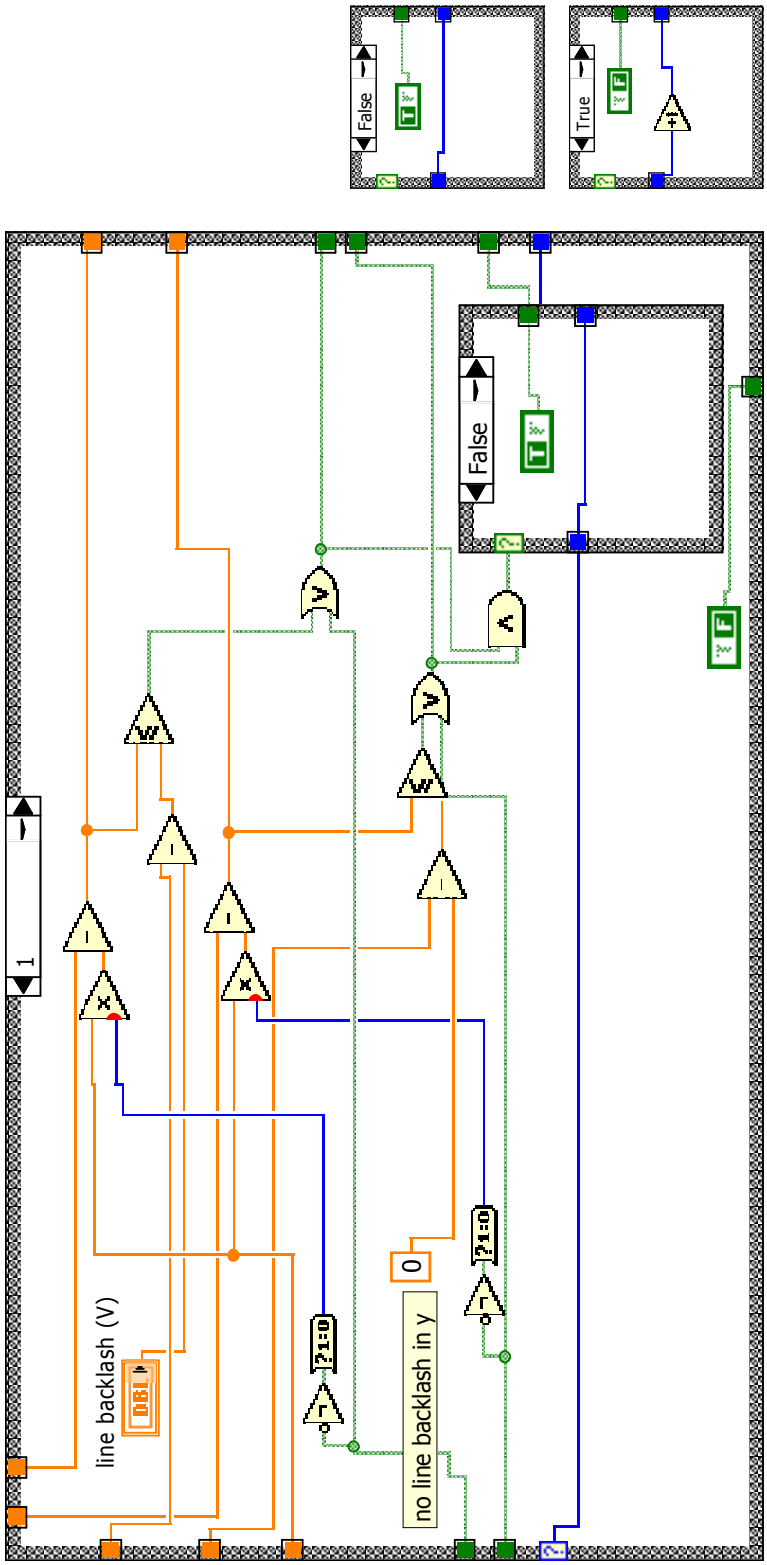
False
True
False
1
line backlash (V)
DBL
I21:0
0
no line backlash in y

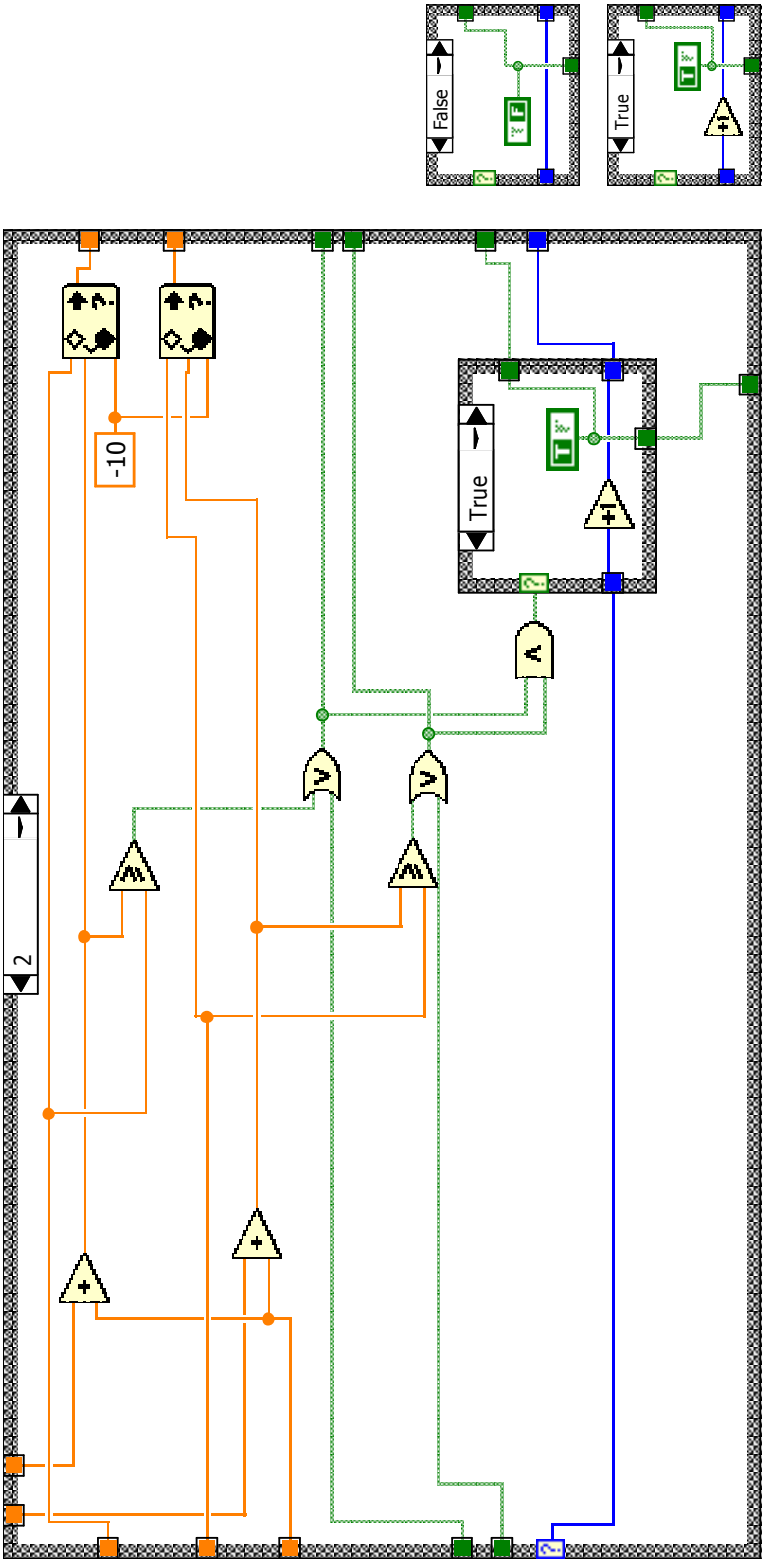
False
True
True
-10
2

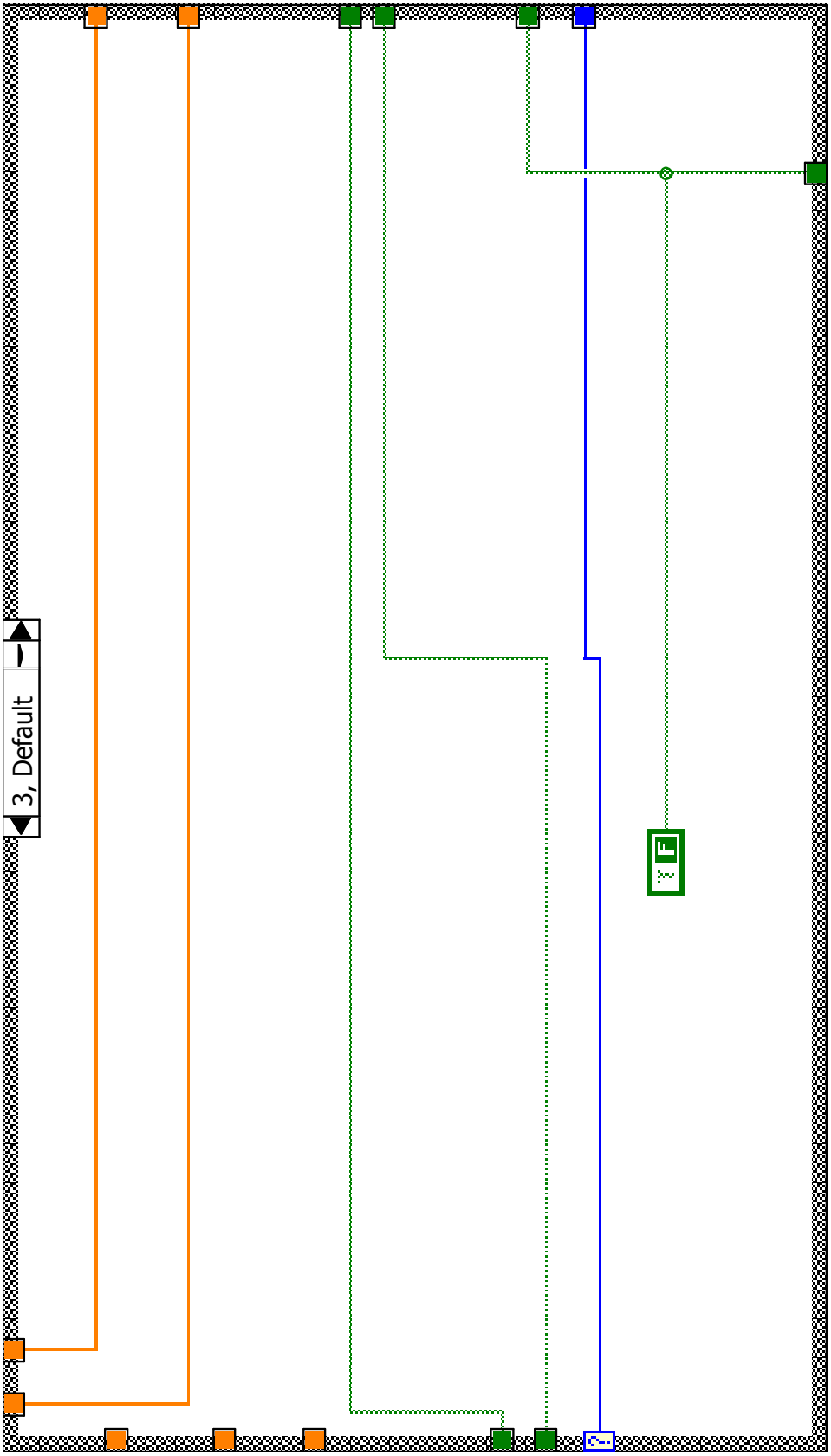
3, Default

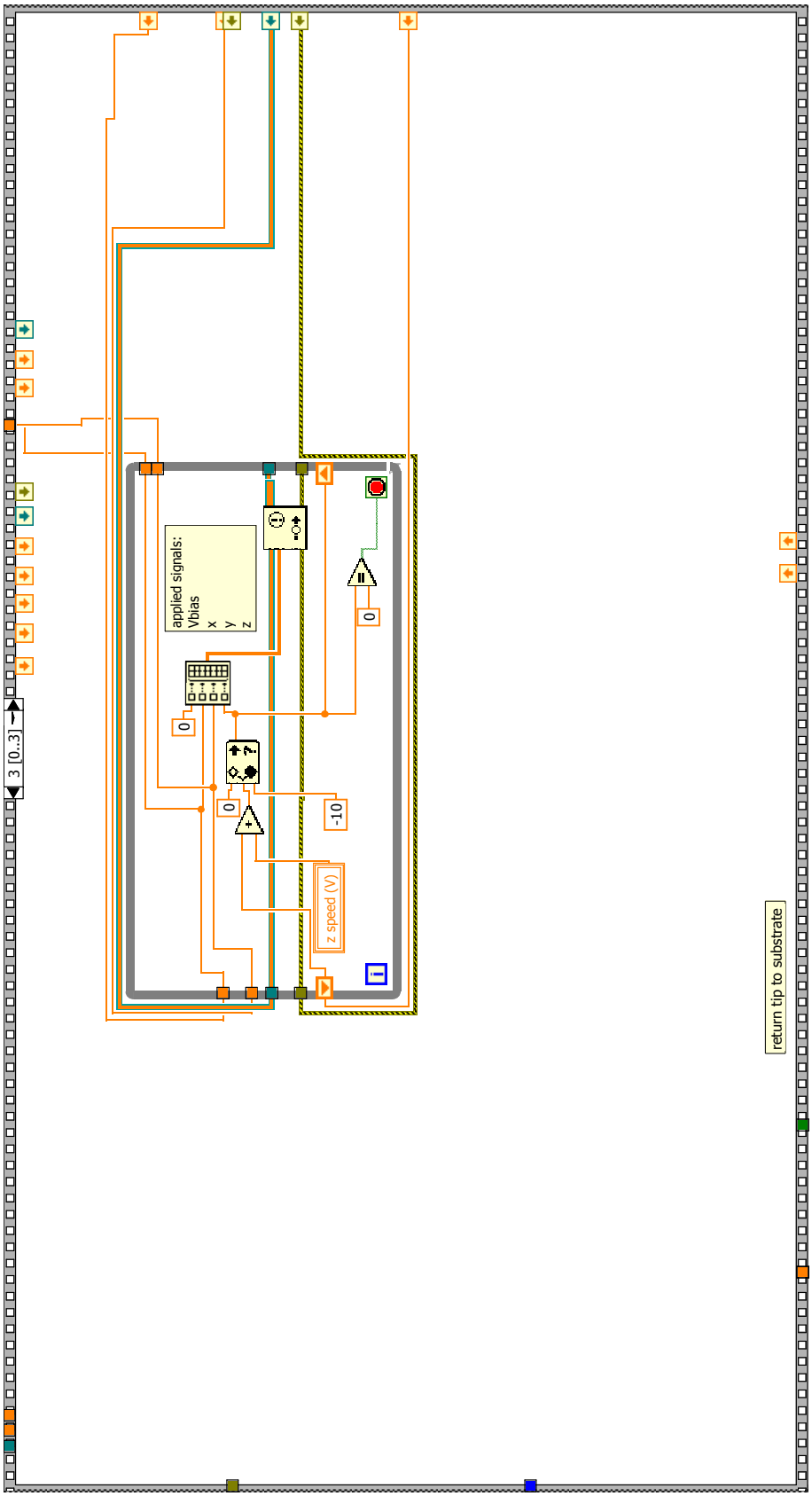
3 [0..3]
applied signals:
Vbias
x
y
z
0
0
0
-10
z speed (V)
return tip to substrate

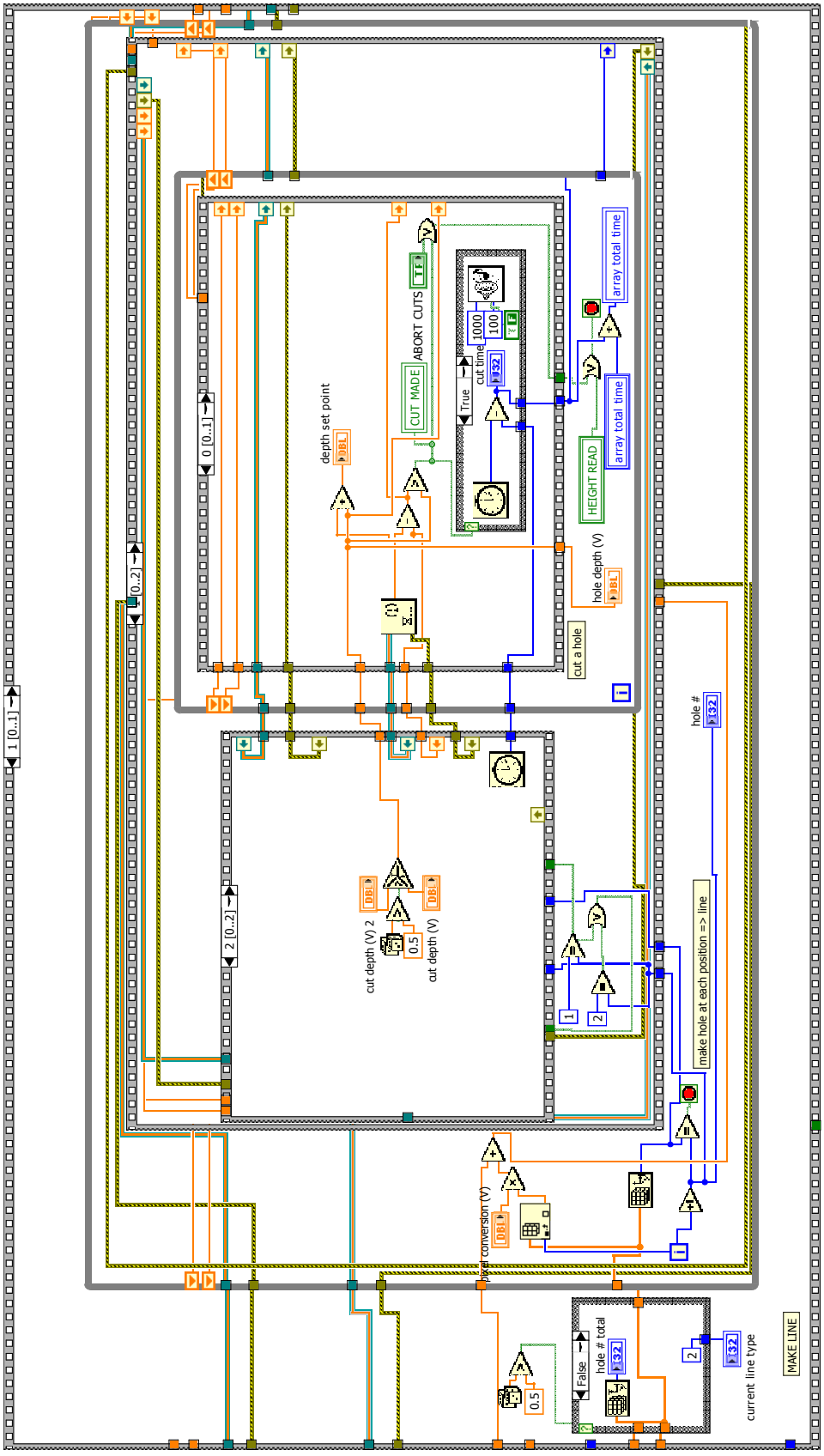
1 [0..1]
0 [0..1]
[0..2]
2 [0..2]
depth set point
CUT MADE
ABORT CUTS
TF
1000
100
cut time
True
array total time
HEIGHT READ
hole depth (V)
cut a hole
hole #
make hole at each position => line
cut depth (V) 2
cut depth (V)
0.5
conversion (V)
hole # total
False
current line type
MAKE LINE

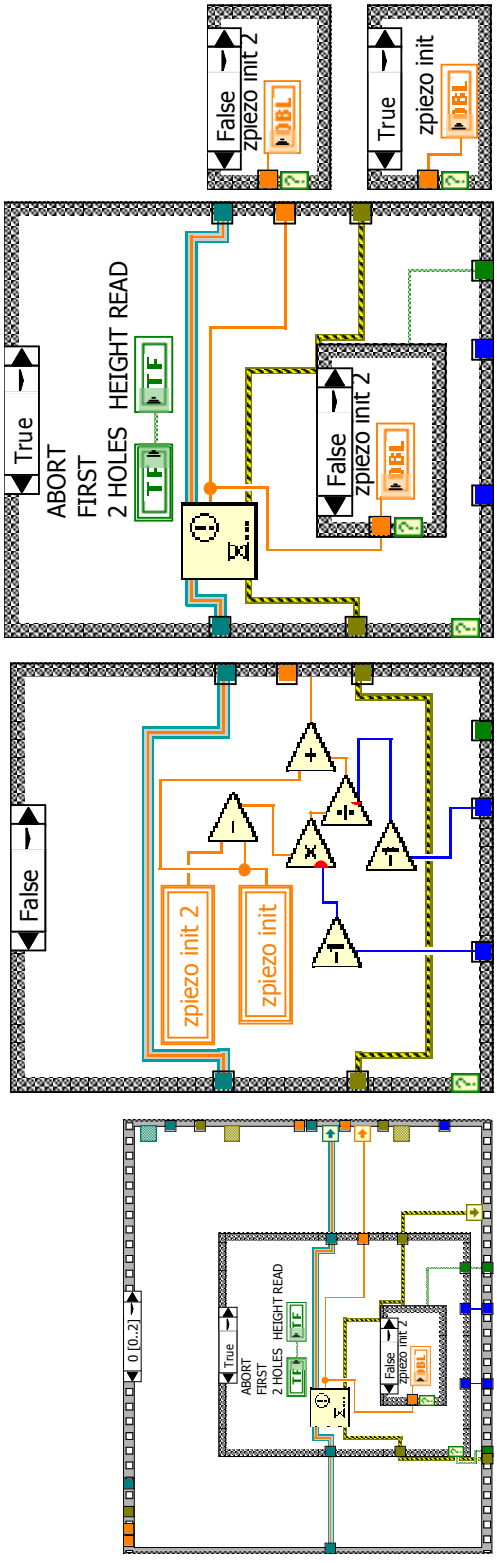
0 [0..2]
True
ABORT
FIRST
2 HOLES
HEIGHT READ
TF
False
zpiezo init 2
DBL
True
zpiezo init
False
zpiezo init 2
zpiezo init

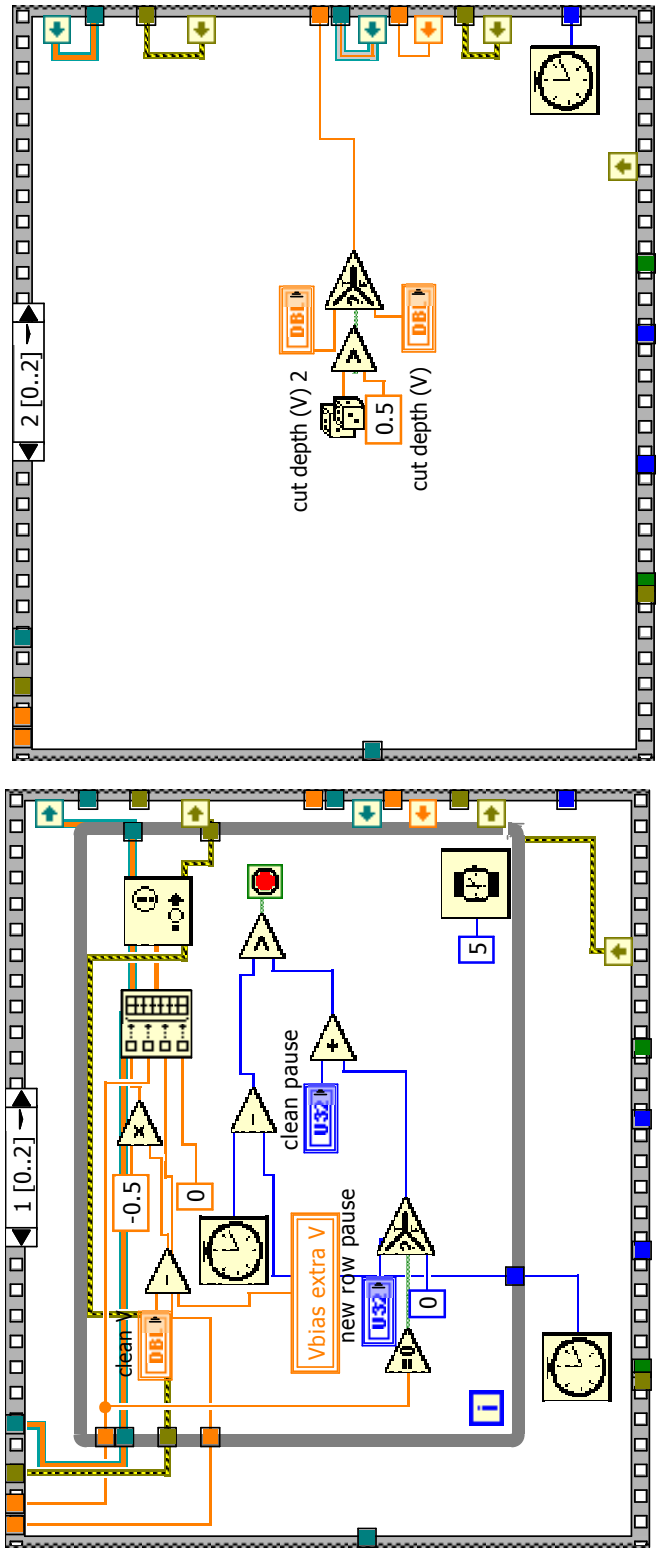
2 [0..2]
cut depth (V) 2
0.5
cut depth (V)
1 [0..2]
clean pause
-0.5
0
clean
Vbias extra V
new rqw pause
5
i

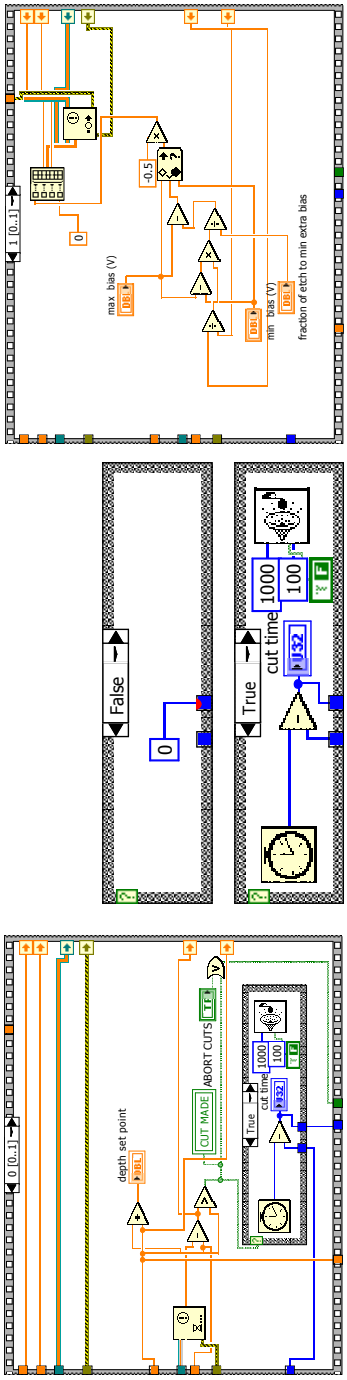
1 [0..1]
0
-0.5
max bias (V)
DBL
min bias (V)
fraction of etch to min extra bias
False
0
True
cut time
1000
100
U32
0 [0..1]
depth set point
CUT MADE
ABORT CUTS
TF

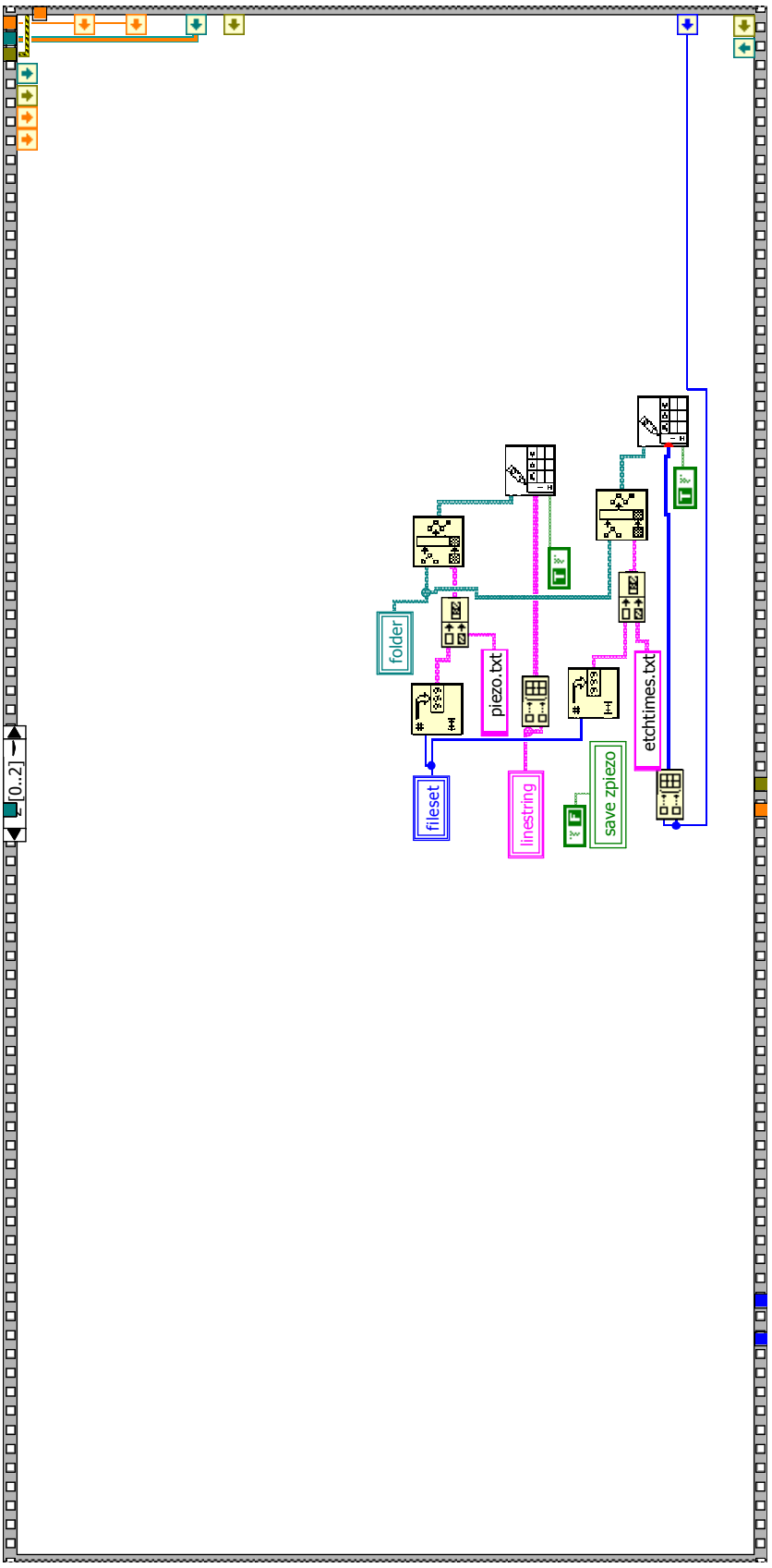
[0..2]
folder
piezo.txt
fileset
linestring
save zpiezo
etchtimes.txt

BIBLIOGRAPHY

[1] L Ci, Z Xu, L Wang, W Gao, F Ding, and K Kelly, "Controlled nanocutting of graphene," *Nano Research*, Jan 2008.

[2] Hugh O Pierson, *Handbook of Carbon, Graphite, Diamond and Fullerenes - Properties, Processing and Applications*, Noyes Publications, Park Ridge, New Jersey, 1993.

[3] Inc./SPI Supplies Structure Probe, "Hopg - highly ordered pyrolytic graphite - spi supplies," web, October 2009.

[4] A K Geim and K S Novoselov, "The rise of graphene," *Nature Materials*, vol. 6, no. 3, pp. 183, Mar 2007.

[5] F Rose, P Martin, H Fujita, and H Kawakatsu, "Adsorption and combing of dna on hopg surfaces of bulk crystals and nanosheets: . . . ," *Nanotechnology*, Jan 2006.

[6] F Rose, A Debray, P Martin, H Fujita, and H Kawakatsu, "Suspended hopg nanosheets for hopg nanoresonator engineering and new carbon nanostructure synthesis," *Nanotechnology*, vol. 17, pp. 5192, Oct 2006.

[7] X Lu, H Huang, N Nemchuk, and R Ruoff, "Patterning of highly oriented pyrolytic graphite by oxygen plasma etching," *Appl. Phys. Lett.*, Jan 1999.

[8] R Windholz and P Molian, "Nanosecond pulsed excimer laser machining of chemical vapour deposited diamond and highly . . . ," *Journal of Materials Science*, Jan 1997.

[9] S Masubuchi, M Ono, K Yoshida, and K Hirakawa, "Fabrication of graphene nanoribbon by local anodic oxidation lithography using atomic force . . . ," *Appl. Phys. Lett.*, Jan 2009.

[10] J Park, C Zhang, R Liang, and B Wang, "Nano-machining of highly oriented pyrolytic graphite using conductive atomic force microscope tips . . . ," *Nanotechnology*, Jan 2007.

[11] A Giesbers, U Zeitler, S Neubeck, and F Freitag, "Nanolithography and manipulation of graphene using an atomic force microscope," *Solid State Communications*, Jan 2008.

[12] L Weng, L Zhang, Y Chen, and L Rokhinson, "Atomic force microscope local oxidation nanolithography of graphene," *Appl. Phys. Lett.*, Jan 2008.

[13] Yan Jiang and Wanlin Guo, "Convex and concave nanodots and lines induced on hopg surfaces by afm voltages in ambient air," *Nanotechnology*, vol. 19, no. 34, pp. 345302, Jul 2008.

[14] T R Albrecht, M M Dovek, M D Kirk, C A Lang, C F Quate, and D P E Smith, "Nanometerscale hole formation on graphite using a scanning tunneling microscope," *Appl. Phys. Lett.*, vol. 55, pp. 1727, 1989.

[15] Robin L Mccarley, Samuel A Hendricks, and Allen J Bard, "Controlled nanofabrication of highly oriented pyrolytic graphite with the scanning tunneling microscope," *J. Phys. Chem.*, vol. 96, no. 25, pp. 10089–10092, Dec 1992.

[16] L C Venema, J W G Wildöer, H L J T Tuinstra, C Dekker, A G Rinzler, and R E Smalley, "Length control of individual carbon nanotubes by nanostructuring with a scanning tunneling microscope," *Appl. Phys. Lett.*, vol. 71, pp. 2629, 1997.

[17] S Kondo, S Heike, M Lutwyche, and Y Wada, "Surface modification mechanism of materials with scanning tunneling microscope," *Journal of Applied Physics*, vol. 78, pp. 155, 1995.

[18] Roland Wiesendanger, *Scanning probe microscopy and spectroscopy : methods and applications*, Cambridge University Press, Cambridge, England, 1994.

[19] C J Roberts, M J Wilkins, G Beamson, M C Daviest, D E Jacksont, P D Scholes, S J B Tendler, and P M Williams, "The demonstration of controlled surface modification achievable with a scanning tunnelling . . . ," *Nanotechnology*, Jan 1992.

[20] P Marella and R Pease, "Comment on "writing nanometerscale symbols in gold using the scanning tunneling microscope"," *Appl. Phys. Lett.*, Jan 1989.

[21] C Wang, C Bai, X Li, G Shang, I Lee, X Wang, X Qiu, and F Tian, "Evidence of diffusion characteristics of field emission electrons in nanostructuring process on graphite surface," *Appl. Phys. Lett.*, vol. 69, pp. 348, 1996.

[22] Dal-Hyun Kim and Ja-Yong Koo, "Cutting of multiwalled carbon nan-

otubes by a negative voltage tip of an atomic force microscope: A possible mechanism," *Phys. Rev. B*, vol. 68, no. 11, Sep 2003.

[23] W Mizutani, J Inukai, and M Ono, "Making a monolayer hole in a graphite surface by means of a scanning tunneling microscope," *Jpn. J. Appl. Phys.*, vol. 29, no. 5, pp. L815–L817, 1990.

[24] M Matsumoto, T Manako, and H Imai, "Electrochemical stm investigation of oxidative corrosion of the surface of highly oriented pyrolytic graphite," *J. Electrochem. Soc.*, vol. 156, no. 10, pp. B1208–B1211, 2009.

[25] M Pourbaix, *Atlas of electrochemical equilibria in aqueous solutions*, National Association of Corrosion Engineers, second edition, 1974.

[26] J Freund, J Halbritter, and J Horber, "How dry are dried samples? water adsorption measured by stm," *Microscopy research and technique*, Jan 1999.

[27] S Stankovich, D Dikin, and R Piner, "Synthesis of graphene-based nanosheets via chemical reduction of exfoliated graphite ...," *Carbon*, Jan 2007.

[28] P S Spinney, S D Collins, and R L Smith, "Solid-phase direct write (spdw) of carbon via scanning force microscopy," *Nano Lett.*, vol. 7, no. 6, pp. 1512–1515, 2007.

[29] J Jang, G C Schatz, and M A Ratner, "How narrow can a meniscus be?," *Phys. Rev. Lett.*, vol. 92, no. 8, pp. 085504, 2004.

[30] A Brett and A Chiorcea, "Atomic force microscopy of dna immobilized onto a highly oriented pyrolytic graphite ...," *Langmuir*, Jan 2003.

[31] A Chiorcea and A Oliveira Brett, "Atomic force microscopy characterization of an electrochemical dna-biosensor," *Bioelectrochemistry*, Jan 2004.

[32] F Rose, A Debray, P Martin, and H Fujita, "Suspended hopg nanosheets for hopg nanoresonator engineering and new carbon ...," *Nanotechnology*, Jan 2006.

[33] M Y Han, B Özyilmaz, Y Zhang, and P Kim, "Energy band-gap engineering of graphene nanoribbons," *Physical review letters*, vol. 98, no. 20, pp. 206805, 2007.